5 Fracture and Fatigue Models for Composites

5.1 Introduction

The effective fatigue model for engineering composites analysis is decisive for a precise estimation of the overall life of this structure and satisfactory reliability analysis of such materials. Various theoretical, experimental and computational criteria must be satisfied in the same time to obtain such a model [37,172,246,298]. These criteria may include material properties of composite constituents [226,258], composite type [229] (ductile or brittle components), spatial distribution, length (continuity) as well as size effect of the reinforcing fibres [219,220,335], frequency effects [350], load amplitude type [48] (constant or not), micromechanical phenomena [110,217,279], etc. First of all, a very precise, experimentally based deterministic idea of fatigue life cycle estimation has to be proposed. It should be adequate for the composite components, the technology applied and numerical methodology implemented. Monitoring of most engineering composites and preventing the fatigue failure is very complicated and usually demands very modern technology [360]. It is widely known that the interface conditions and phenomena can be decisive factors for both static fracture and fatigue resistance of laminates, fibre− and particle−reinforced composites. Analytical models even in the case of linear elasticity models are complicated [369], therefore numerical analysis is very popular in this area. Engineering FEM software makes it possible to simulate delamination processes [362] and fatigue damage [62,277] in fibre−reinforced composites as well as time−dependent interlaminar debonding processes [69], for instance.

The application of the well−known Palmgren−Miner or Paris−Erdogan laws is not always recommended as the most effective method in spite of their simplicity or wide technological usage. The choice of fatigue theory should be accompanied with a corresponding sensitivity analysis, where physical and material input parameters included into the fatigue life cycle equation are treated as design variables. Due to the sensitivity gradients determination, the most decisive parameters should be considered, while the remaining ones, considering further stochastic analysis complexity, may be omitted. The sensitivity gradients can be determined analytically using symbolic computation packages (MAPLE, MATLAB, MATHEMATICA, etc.) or may result from discrete FEM computations, for instance. A related problem is to decide if the local concept of composite fatigue is to be applied (critical element concept, for instance), where local fatigue damage causes global structural changes of the composite reliability. This results in computational FEM or Boundary Element Method (BEM) based analyses of the whole composite in its real configuration, including the microgeometry and all interface phenomena into it. Alternatively, the homogenisation method can be applied, where the complementary energy or potential energy of the entire system is the only measure of composite fatigue. Then, the global discretisation of the original structure is used instead and the equivalent, homogeneous medium is simulated numerically.

Next, an appropriate analytical or computational stochastic analysis method corresponding to the level of randomness of input parameters is considered. The Monte Carlo simulation based analysis, stochastic second or third order perturbation method or, alternatively, stochastic spectral analysis can be taken into account. The first method does not have any restrictions on input random variable probabilistic moment interrelations. However, time consuming computations can be expected. Numerical analysis using the second approach implementation is very fast, but not sufficiently effective for larger than 10% variations of input random parameters, while the last approach has some limitations on convergence of the output parameters and fields. The choice between the methods proposed is implied by the availability of the experimental techniques, considering the input randomness level. On the other hand this choice is determined by relevant reliability criteria for composites. Furthermore, having collected most of the deterministic fatigue concepts for composites, corresponding stochastic equations can be obtained automatically using analytical derivation or computer simulation techniques.

Combination of deterministic models and stochastic methods requires another engineering decision about the choice of the randomness type to be analysed. It is known from recent references in this area that (i) random variables, (ii) random fields as well as (iii) stochastic processes can be considered as the input of the entire fatigue analysis. According to the state−of−the−art research, the first two types of randomness can be considered together with FEM or BEM based computational simulation, while the stochastic processes can be used in terms of direct simulation of the fatigue process when the analytical solution is known. Some approximate methods of combining discrete modelling with stochastic degradation of homogeneous materials are available in reliability modeling; however without any application in engineering composites area until now.

Various fatigue models worked out for composites can be classified in different ways: using the scale of the model application (local or global) or considering the main goal of the analysis (fatigue cycle number, its stiffness reduction, its crack growth or damage function determination), the analysis type (deterministic, probabilistic or stochastic) as well as the composite material type (ceramic, polymer−based, metal matrix and so forth).

Considering various scales of engineering composites and fatigue phenomena related to them, the local and, alternatively, global approaches are considered. Local and microlocal models represented by the critical element concept [299], assume that there exists so−called critical element in the entire composite structure that controls the total fatigue damage (as well as subcrtitical elements, too), and then the local damage is governing the reliability of the whole composite structure.

This assumption results in the fact that the whole composite, together with microstructural defects increasing during fatigue processes, should be discretised for the FEM or BEM simulation. Taking into account the application of the probabilistic analysis, the model implies the randomness in microgeometry of the composite, which is extremely difficult in computational simulation, as is shown below. Some special purpose algorithms are introduced to replace the randomness in composite interface geometry with the stochasticity of material thermoelastic properties.

Alternatively, a homogenisation method is proposed for more efficient fracture and fatigue phenomena analysis [223] that originated from analysis of linear periodic elastic composites without defects. The main idea is to find the medium equivalent to the original composite in terms of complementary energy, or potential energy, equal for both media. The final goal of the homogenisation procedure is to find the effective material characteristics defining the equivalent homogeneous medium. The effective constitutive relations can be found for the composite with elastic, elastoplastic or even viscoelastoplastic components with and/or without microstructural defects. The general assumption of the model means, however, that every local phenomenon can be averaged in some sense in the entire composite volume and that the global, not local, phenomena result in the overall composite fatigue.

5.2 Existing Techniques Overview

Taking into account the results of fatigue analysis, four essentially different approaches can be observed: (i) direct determination of the fatigue cycle number N, (ii) fatigue stiffness reduction where mechanical properties of the composite are decreased in the function of N, (iii) observation of the crack length growth a as a function of fatigue cycle number (as da/dN, taking into account the physical nature of fatigue phenomenon) or, alternatively, (iv) estimation of the damage function in terms of dD/dN. A damage function is usually proposed as follows:

(1) D=0 with cycle number n=0;

(2) D=1, where failure occurs;

(3) $D=\sum_{i=1}^{n}\Delta D_i$, where ΔD_i is the amount of damage accumulation during fatigue at stress level r_i. Generally, the function D can be represented as

$$D = D(n, r, f, T, M, ...) \tag{5.1}$$

where n indexes a number of the current fatigue cycle, r is the applied stress level, f denotes applied stress frequency, T is temperature, while M denotes the moisture content. Then, contrary to the crack length growth analysis, the damage function can be proposed each time in a different form as a function of various structural parameters.

Let us note that direct determination of fatigue cycle number makes it possible to derive, without any further computational simulations, the life of the structure till the failure, while the stiffness reduction approach is frequently used together with the FEM or BEM structural analyses. The crack length growth and damage function approach are used together with the structural analysis FEM programs, usually to compute the stress intensity factors. However final direct or symbolic integration of crack length or damage function is necessary to complete the entire fatigue life computations.

Considering the mathematical nature of the fatigue life cycle estimation, the deterministic approach can be applied, where all input parameters are defined uniquely by their mean values. Otherwise, the whole variety of probabilistic approaches can be introduced where fatigue structural life is described as a simple random variable with structural parameters defined deterministically and random external loads. The cumulative fatigue damage can be treated as a random process, where all design parameters are modelled as stochastic parameters. However, in all probabilistic approaches sufficient statistical information about all input parameters is necessary, which is especially complicated in the last approach where random processes are considered due to the statistical input in some constant periods of time (using the same technology to assure the same randomness level).

The analysis of fatigue life cycle number begins with direct estimation of this parameter by a simple power function (A5.1) consisting of stress amplitude as well as some material constant(s). Alternatively, an exponential−logarithmic equation can be proposed (A5.2), where temperature, strength and residual stresses are inserted. Both of them have a deterministic form and can be randomised using any of the methods described below. The weak point is the homogeneous character of the material being analysed; to use these criteria for composites, the effective parameters should be calculated first. In contrary to theoretical models, the experimentally based probabilistic law can be proposed where parameters of the Weibull distribution of static strength are inserted (A5.3); it is important to underline that this law does not have its deterministic origin.

More complicated from the viewpoint of engineering practice are the stiffness reduction models (cf. A5.4−A5.7), where structural material characteristics are reduced together with a successive fatigue cycle number increase. The stiffness reduction model is used in FEM or BEM dynamical modelling to recalculate the component stiffness in each cycle. It is done using a linear model for stiffness reduction, cf. (A5.5), as well as some power laws (see (A5.4), for example) determined on the basis of mechanical properties reduction rewritten for homogeneous media only. An alternative power law presented as (A5.7) consists of the time of rupture, creep and fatigue, measured in hours. Considering the random analysis aspects, a probabilistic treatment of material properties seems to be much more justified.

Deterministic fatigue crack growth analysis presented by (A5.8) − (A5.29) can be classified taking into account the physical basis of this law formation, such as energy approaches (A5.8) − (A5.11), crack opening displacement (COD) based approaches (A5.12), (A5.15) − (A5.17), (A5.19) and (A5.20), continuous dislocation formalism (A5.13), skipband decohesion (A5.18), nucleation rate process models (A5.14) and (A5.15), dislocation approaches (A5.23) and (A5.24), monotonic yield strength dependence (A5.25) and (A5.31) as well as another mixed laws (A5.26) – (A5.30) and (A5.32) – (A5.35). Description of the derivative da/dN enables further integration and determination of the critical crack length. The second classification method is based on a verification of the validity of a particular theory in terms of elastic (A5.8) – (A5.20), (A5.26) – (A5.30), (A5.32) – (A5.34) or elastoplastic (A5.22) – (A5.25) and (A5.31) mechanism of material fracture. Most of them are used for composites, even though they are defined for homogeneous media, except for the Ratwani–Kan and Wang–Crossman models (A5.21) and (A5.22), where composite material characteristics are inserted. All of the homogeneous models contain stress intensity factor ΔK in various powers (from 2 to n), while composite–oriented theories are based on delamination length parameter. The structure of these equations enables one to include statistical information about any material or geometrical parameters and, next, to use a simulation or perturbation technique to determine expected values and variances of the critical crack length, which are very useful in stochastic reliability analysis.

An essentially different methodology is proposed for the statistical analysis [9,35,130,288,333,349,359] and in the stochastic case [241,244,373], where the crack size and/or components material parameters, their spatial distribution may be treated as random processes (cf. eqns (A5.36) – (A5.44)). Then, various representations and types of random fields and stochastic processes are used, such as stationary and nonstationary Gaussian white noise, homogeneous Poisson counting process [204] as well as Markovian [304], birth and death or renewal processes. However all of them are formulated for a globally homogeneous material. These methods are intuitively more efficient in real fatigue process modelling than deterministic ones, but they require definitely a more advanced mathematical apparatus. Further, randomised versions of deterministic models can be applied together with structural analysis programs, while stochastic characters of a random process cannot be included without any modification in the FEM or the BEM computer routines. An alternative option for stochastic models of fatigue is experimentally based formulation of fatigue law, where measurements of various material parameters are taken in constant time periods. Then, statistical information about expected values and higher order probabilistic characteristics histories is obtained, which allows approximation of the entire fatigue process. Such a method, used previously for homogeneous structural elements, is very efficient in stochastic reliability prognosis and then random fatigue process can be included in SFEM computations. Let us observe that formulations analogous to the ones presented above can be used for ductile fracture of composites where initiation, coalescence and closing of microvoids are observed under periodic or quasiperiodic external loads.

A wide variety of fatigue damage function models is collected at the end of the appendix. The basic rules are based on the numbers of cycles to failure ((A5.45) – (A5.48), (A5.54) – (A5.57), (A5.63) – (A5.65) and (A5.67)) illustrated with classical and modified Palmgren–Miner approach, for instance. This variable is most frequently treated as a random variable or a random process in stochastic modelling. Another group consists of mechanical models, where stress (A5.50) – (A5.53) or strain (A5.66) – (A5.67) limits are used instead of global life cycle number. Such models reflect the actual state of a composite during the fatigue process better and are more appropriate for the needs of computational probabilistic structural analysis. The combination of both approaches is proposed by Morrow in (A5.66) for constant stress amplitude and for different cycles by (A5.67). The overall fatigue analysis is then more complicated. However the most realistic model is obtained. Accidentally, Fong model is used, where damage function is represented by an exponential function of damage trend k, which is a compromise between counting fatigue cycles and mechanical tensor measurements.

The very important problem is to distinguish the scale of application of the proposed model, especially in the context of determination of a fatigue crack length. The models valid for long cracks do not account for the phenomena appearing at the microscale of the composite specimen. On the contrary, cf. (A5.33), the microstructural parameter d is introduced, which makes it possible to include material parameters in the microscale in the equation describing the fatigue crack growth.

All the models for the damage function can be extended on random variables theoretically, by perturbation methodology, or computationally, using the relevant MCS approach. The essential minor point observed in most of the formulae described above is a general lack of microstructural analysis. The two approaches analysed above can model cracks in real laminates, while other types of composites must be analysed using fatigue laws for homogeneous materials. This approach is not a very realistic one, since fatigue resistance of fibres, matrices, interfaces and interphases is essentially different. Considering the delamination phenomena during periodic stress changes, an analogous fatigue approach for fibre–matrix interface decohesion should be worked out. The probabilistic structural analysis of such a model can be made using SFEM computations or by a homogenisation. However a closed-form fatigue law should be completed first.

As is known, there exist a whole variety of effective probabilistic methods in engineering. The usage of any of these approaches depends on the following factors: (a) type of random variables (normal, lognormal or Weibull, for instance), (b) probabilistic information on the input random variables, fields or processes (in the form of moments or probability density function (PDF)), (c) interrelations between particular probabilistic characteristics of the input (of higher to the first order, especially), (d) method of solution of corresponding deterministic problem and (e) available computational time as well as (f) applied reliability criteria.

If the closed form solution is available or can be derived symbolically using computational algebra, then the probability density function (PDF) of the output can be found starting from analogous information about the input PDF. It can be done generally from definition – using integration methods, or, alternatively, by the characteristic function derivation. The following PDF are used in this case:

lognormal for stress and strain tensors, lognormal and Gaussian distributions for elastic properties as well as for the geometry of fatigue specimen. Weibull density function is used to simulate external loads (shifted Rayleigh PDF, alternatively), yield strength as well as the fracture toughness, while the initial crack length is analysed using a shifted exponential probability density function.

As is known [313], one of the following computational methods can be used in probabilistic fatigue modelling: Monte Carlo simulation technique, stochastic (second or higher order) perturbation analysis as well as some spectral techniques (Karhunen−Loeve or polynomial chaos decompositions). Alternatively, Hermitte−Gauss quadratures (HGQ) or various sampling methods (Latin Hypercube Sampling – LHS, for instance) in conjunction with one of the latters may be used. Computational experience shows that simulation and sampling techniques are or can be implemented as exact methods. However their time cost is very high. Perturbation-based approaches have their limitations on higher order probabilistic moments, but they are very fast. The efficiency of spectral methods depends on the order of decomposition being used, but computational time is close to that offered by the perturbation approach. Unfortunately, there is no available full comparison of all these techniques – comparison of MCS and SFEM can be found in [208], HGQ with SFEM in [237] and stochastic spectral FEM with MCS in [113,114]. A lot of numerical experiments have been conducted in this area, including cumulative damage analysis of composites by the MCS approach (Ma *et al.* [243]) and simulation of stochastic processes given by (A5.30) − (A5.38). However, the problem of an appropriate conjunction of stochastic processes and structural analysis using FEM or BEM techniques has not been solved yet.

Let us analyse the application of the perturbation technique to damage function D extension, where it is a function of random parameter vector b. Using a stochastic Taylor expansion it is obtained that

$$D(\mathbf{b}) = D^0\left(\mathbf{b}^0\right) + \varepsilon \Delta b^r D^{,r}\left(\mathbf{b}^0\right) + \tfrac{1}{2}\varepsilon^2 \Delta b^r \Delta b^s D^{,rs}\left(\mathbf{b}^0\right) \tag{5.2}$$

Then, according to the classical definition, the expected value of this function can be derived as

$$\begin{aligned} E[D(\mathbf{b})] &= \int_{-\infty}^{+\infty} D(\mathbf{b})\; p(\mathbf{b})\; d\mathbf{b} \\ &= \int_{-\infty}^{+\infty} \left(D^0\left(\mathbf{b}^0\right) + \varepsilon \Delta b^r D^{,r}\left(\mathbf{b}^0\right) + \tfrac{1}{2}\varepsilon^2 \Delta b^r \Delta b^s D^{,rs}\left(\mathbf{b}^0\right)\right) p(\mathbf{b})\; d\mathbf{b} \\ &= D^0\left(\mathbf{b}^0\right) + \tfrac{1}{2} D^{,rs}\left(\mathbf{b}^0\right) Cov\left(b^r, b^s\right) \end{aligned} \tag{5.3}$$

while variance is

$$Var(D) = \left(\frac{\partial D}{\partial \mathbf{b}}\right)^2 Var(\mathbf{b}) \tag{5.4}$$

Since this function is usually used for damage control, which in the deterministic case is written as $D \leq 1$, an analogous stochastic formulation should be proposed. It can be done using some deterministic function being a combination of damage function probabilistic moments as follows:

$$D(\mathbf{b}) \leq g(\mu_k[D(\mathbf{b})]) \leq 1 \tag{5.5}$$

where $\mu_k(D(\mathbf{b}))$ denote some function of up to kth order probabilistic moments. Usually, it is carried out using a stochastic 'envelope' function being the upper bound for the entire probability density function as, for instance

$$g(\mu_k[D(\mathbf{b})]) = E[D(\mathbf{b})] - 3\sqrt{D(\mathbf{b})} \tag{5.6}$$

This formula holds true for Gaussian random deviates only. It should be underlined that this approximation should be modified in the case of other random variables, using the definition that the value of damage function should be smaller than 1 with probability almost equal to 1; the lower bound can be found or proposed analogously. In the case of classical Palmgren−Miner rule (A5.45), with fatigue life cycle number N treated as an input random variable,

$$D = \frac{n}{N}, \qquad N \equiv b \tag{5.7}$$

the expected value is derived as follows [215]:

$$E[D] = D^0 + \tfrac{1}{2} D^{,NN} Var(N) = \frac{n}{N^0} + \frac{n}{(N^0)^3} Var(N) \tag{5.8}$$

and the variance in the form of

$$Var(D) = (D^{,N})^2 Var(N) = \frac{n^2}{(N^0)^4} Var(N) \tag{5.9}$$

It is observed that the methodology can also be applied to randomise all of the functions D listed in the appendix to this chapter with respect to any single or any vector of composite input random parameters. In contrast to the classical derivation of the probabilistic moments from their definitions, there is no need to make detailed assumptions on input PDF to calculate expected values and variances for the inversed random variables in this approach.

Let us determine for illustration the number of fatigue cycles of cumulative damage of a crack at the weld subjected to cyclic random loading with the specified expected value and standard deviation (or another second order probabilistic characteristics) of $\Delta\sigma$. Let us assume that the crack in a weld is growing according to the Paris–Erdogan law, cf. (A5.26), described by the equation

$$\frac{da}{dN} = C\left(Y\Delta\sigma\sqrt{\pi}\right)^m a^{\frac{m}{2}} \tag{5.10}$$

and that $Y \neq Y(a)$. Then

$$\int \frac{da}{a^{\frac{m}{2}}} = \int C\left(Y\Delta\sigma\sqrt{\pi}\right)^m dN \tag{5.11}$$

which gives by integration that

$$\frac{1}{-\frac{m}{2}+1} a^{-\frac{m}{2}+1} = C\left(Y\Delta\sigma\sqrt{\pi}\right)^m N + D, \quad D \in \Re \tag{5.12}$$

Taking for N=0 the initial condition $a=a_i$, it is obtained that

$$\left(\frac{a}{a_i}\right)^k = \frac{1}{1-\beta N} \tag{5.13}$$

for

$$\kappa = \frac{m}{2} - 1, \quad \beta = \kappa a_i^{\kappa} C\left(Y\Delta\sigma\sqrt{\pi}\right)^m \tag{5.14}$$

Therefore, the number of cycles to failure is given by

$$N_f = \frac{1}{\beta} \tag{5.15}$$

The following equation is used to determine the probabilistic moments of the number of cycles for a crack to grow from the initial length a_i to its final length a_f:

$$\Delta N = \int_{a_i}^{a_f} \frac{1}{C(\Delta K)^m} da \tag{5.16}$$

Substituting for ΔK one obtains

$$\Delta N = \frac{1}{C(\Delta\sigma)^m \pi^{\frac{m}{2}}} \int_{a_i}^{a_f} \frac{1}{Y^m a^{\frac{m}{2}}} da \tag{5.17}$$

By the use of a stochastic second order perturbation technique we determine the expected value of ΔN as

$$E[\Delta N] = \Delta N(\Delta\sigma^0) + \frac{1}{2}\frac{\partial^2(\Delta N(\Delta\sigma^0))}{\partial(\Delta\sigma^0)^2} Var(\Delta\sigma) \tag{5.18}$$

and the variance of number of cycles as

$$Var(\Delta N) = \left(\frac{\partial(\Delta N(\Delta\sigma^0))}{\partial(\Delta\sigma^0)}\right)^2 Var(\Delta\sigma) \tag{5.19}$$

Adopting m=2 it is calculated using (5.17) and (5.18) that

$$E[\Delta N] = \frac{1}{CY^2\pi}\ln\left(\frac{a_f}{a_i}\right)\left[\frac{1}{E^2[\Delta\sigma]} + \frac{6}{E^4[\Delta\sigma]}Var(\Delta\sigma)\right] \tag{5.20}$$

and

$$Var(\Delta N) = \frac{4}{C^2Y^4\pi^2}\ln^2\left(\frac{a_f}{a_i}\right)\frac{\alpha(\Delta\sigma)}{E^4[\Delta\sigma]} \tag{5.21}$$

The following data are adopted in probabilistic symbolic computations: $E[\Delta\sigma] = \sigma_{max} - \sigma_{min} = 10.0\,MPa$, a_i=25 mm and obtained experimentally C=1.64x10^{-10}, Y=1.15. The visualisation of the first two probabilistic moments of fatigue cycle number is done using the symbolic computation program MAPLE as functions of the coefficient of variation $\alpha(\Delta\sigma)$ and the final crack length a_f. The results of the analysis in the form of deterministic values, corresponding expected values and standard deviations are presented below with the design parameters marked on the horizontal axes.

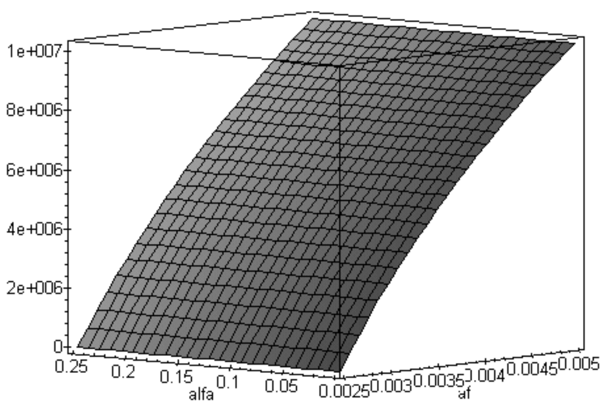

Figure 5.1. Deterministic values of fatigue cycles (dN)

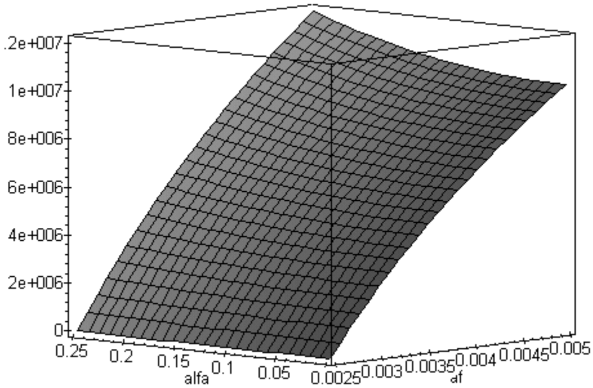

Figure 5.2. Expected values of fatigue cycles number (*EdN*)

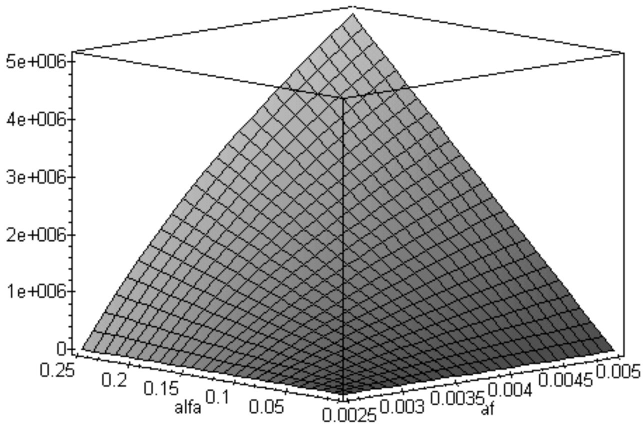

Figure 5.3. Standard deviations of fatigue cycles number (σdN)

Especially interesting here is a comparison between deterministic analysis and expected values obtained for analogous input data. It is seen that the expectations are essentially greater than the deterministic output, which results from (5.17), for instance. The difference increases nonlinearly together with an increase in the coefficient of variation of the stress amplitude $\Delta\sigma$. In the case of $\alpha(\Delta\sigma)$=25% this difference is equal to about 20% of the relevant deterministic values. This result can be used as the safety factor which could be proposed for deterministic analysis as S=1.2 for an analogous range of random variability of the stress amplitude. Furthermore, it is seen that the final crack length is remarkably more decisive for fatigue cycle number (even in a random case) than the coefficient of variation of the stress amplitude.

As shown in Figure 5.3, the variability of the examined standard deviation of $\Delta\sigma$ is essentially different from that typical for deterministic and expected values. The influences of final crack length and input coefficient of variation are almost the same for 25% increases of both parameters. Considering the above it can be concluded that the influence of the random character in fatigue cycle number is important in higher than first order probabilistic moments computations. It is clear that the presented symbolic computation methodology can be next exploited in the determination of stochastic sensitivity gradients of probabilistic moments of the fatigue cycle number with respect to particular random characteristics of the chosen input variables appearing in the fatigue life cycles formula. In particular, it will enable us to compare the sensitivity of various fatigue models with respect to the same parameters in which the sensitivity gradients are the most reasonable and realistic. The situation would be definitely more complicated if the variation of stress amplitude together with fatigue cycle number is analysed. Random fluctuations of $\Delta\sigma$ in time should be taken into account in this case and, therefore, $\Delta\sigma(\omega)=\Delta\sigma(\omega,t)$ is to be considered as a resulting nonstationary random process.

5.3 Computational Issues

Since the deterministic equations are valid for the Monte Carlo simulation analysis as well, then the essential theoretical differences are observed in the case of perturbation based analysis. The corresponding fatigue−oriented SFEM model begins with the new description of the material properties, where the stiffness reduction approach can result in the following equations for the Young modulus, Poisson ratio and material density as well as spring stiffness for interface modelling

$$\begin{aligned} e(n) &= e_0\big(1-D(n)\big),\ \nu(n)=\nu_0\big(1-D(n)\big) \\ \rho(n) &= \rho_0\big(1-D(n)\big),\ k(n)=k_0\big(1-D(n)\big) \end{aligned} \tag{5.27}$$

Therefore, the first two probabilistic moments for the Young modulus can be represented as

$$E[e(n)] = E[e_0]\big(1-E[D(n)]\big) \tag{5.28}$$

$$Var(e(n)) = Var\big(e_0\big(1-D(n)\big)\big) = Var(e_0)\,Var\big(1-D(n)\big) \tag{5.29}$$

and up to the second order perturbation equations are rewritten in the incremental formulation as follows:

- zeroth order

$$M^0_{\alpha\beta}(n)\Delta\ddot{q}^0_\beta(n) + C^0_{\alpha\beta}(n)\Delta\dot{q}^0_\beta(n) + K^0_{\alpha\beta}(n)\Delta q^0_\beta(n) = \Delta Q^0_\alpha(n) \tag{5.30}$$

- first order

$$
\begin{aligned}
& M^{0}_{\alpha\beta}(n)\Delta\ddot{q}^{,r}_{\beta}(n) + C^{0}_{\alpha\beta}(n)\Delta\dot{q}^{,r}_{\beta}(n) + K^{0}_{\alpha\beta}(n)\Delta q^{,r}_{\beta}(n) = \Delta Q^{,r}_{\alpha}(n) + \\
& \quad - \left(M^{,r}_{\alpha\beta}(n)\Delta\ddot{q}^{0}_{\beta}(n) + C^{,r}_{\alpha\beta}(n)\Delta\dot{q}^{0}_{\beta}(n) + K^{,r}_{\alpha\beta}(n)\Delta q^{0}_{\beta}(n) \right)
\end{aligned}
\tag{5.31}
$$

- second order

$$
\begin{aligned}
& M^{0}_{\alpha\beta}(n)\Delta\ddot{q}^{(2)}_{\beta}(n) + C^{0}_{\alpha\beta}(n)\Delta\dot{q}^{(2)}_{\beta}(n) + K^{0}_{\alpha\beta}(n)\Delta q^{(2)}_{\beta}(n) \\
& = \left\{ \Delta Q^{,rs}_{\alpha}(n) - \left(M^{,rs}_{\alpha\beta}(n)\Delta\ddot{q}^{0}_{\beta}(n) + C^{,rs}_{\alpha\beta}(n)\Delta\dot{q}^{0}_{\beta}(n) + K^{,rs}_{\alpha\beta}(n)\Delta q^{0}_{\beta}(n) \right) \right. \\
& \left. - \left(M^{,r}_{\alpha\beta}(n)\Delta\ddot{q}^{,s}_{\beta}(n) + C^{,r}_{\alpha\beta}(n)\Delta\dot{q}^{,s}_{\beta}(n) + K^{,r}_{\alpha\beta}(n)\Delta q^{,s}_{\beta}(n) \right) \right\} \\
& Cov\left(b^{r}(n), b^{s}(n) \right)
\end{aligned}
\tag{5.32}
$$

where the stiffness matrix perturbation orders are defined as

$$
\begin{aligned}
& K^{(.)}_{\alpha\beta}(n) = {}^{(con)}K^{(.)}_{\alpha\beta}(n) + {}^{(\sigma)}K^{(.)}_{\alpha\beta}(n) = \\
& = \int_{\Omega} C^{(.)}_{ijkl}(n) B_{ij\alpha} B_{kl\beta}\, d\Omega + \int_{\Omega} \sigma_{ij}(n-1)\varphi_{k\alpha,i}\varphi_{k\beta,j}\, d\Omega
\end{aligned}
\tag{5.33}
$$

so the dynamical structural response is given in the form

$$
\Delta\ddot{q}^{(.)}_{\beta} = \ddot{q}^{(.)}_{\beta}(n+1) - \ddot{q}^{(.)}_{\beta}(n)
\tag{5.34}
$$

The situation is more complicated when the crack phenomenon is considered apart from the material stochasticity and nonlinearity. In such a situation so−called direct methods are used or special purpose enriched finite elements with crack tip modelling can be applied alternatively. In the latter case, the displacements near the crack tip can be defined as

$$
\begin{cases}
u = K_I f_u + K_{II} g_u \\
v = K_I f_v + K_{II} g_v
\end{cases}
\tag{5.35}
$$

while the near field component f_u can be rewritten as

$$
\begin{aligned}
& f_u = \frac{1}{4G}\sqrt{\frac{r}{2\pi}} \\
& \left\{ \cos\phi \left[(2\gamma - 1)\cos\frac{\theta}{2} - \cos\frac{3\theta}{2} \right] - \sin\phi \left[(2\gamma + 1)\sin\frac{\theta}{2} - \sin\frac{3\theta}{2} \right] \right\}
\end{aligned}
\tag{5.36}
$$

where ϕ denotes the orientation angle of a crack, which is measured from the positive x axis, r and θ are polar coordinates with origin at the crack tip and measured from the crack angle, G is shear modulus, while γ denotes $\gamma = 3 - 4\nu$ for plane strain problems or is equal to $\gamma = \frac{3-\nu}{1+\nu}$ for the plane stress analyses. The corresponding SFEM equations for displacements near the crack tip are rewritten using (5.36), while the stress intensity factors are computed using BEM or FEM techniques or, alternatively, are derived mathematically starting from stress equilibrium and displacement compatibility equations. The numerical results of SFEM analysis for composites with and/or without interface and volumetric microdefects are presented in [193,194], while in the case of the cracked medium they can be found in [33].

Alternatively, the structural microdefects are modelled by spherical voids during the ductile type fatigue fracture. Let us assume that the total number of the microdefects is equal to M_a, their radius is denoted by R_a in the composite component indexed with a. Adopting further that both of them are functions of the fatigue cycle, the modified elasticity tensor components can be calculated using stiffness reduction of the Young modulus and Poisson ratio as follows:

$$
\begin{aligned}
C^{(eff)}_{ijkl(a)}(n) &= \left(1 - \frac{\pi M_a(n) R_a^2(n)}{\Omega_a}\right) E_a(n) \\
&\times \left\{ \frac{\left(1 - \frac{\pi M_a(n) R_a^2(n)}{\Omega_a}\right)\nu_a(n)}{\left[\left(1 + \left(1 - \frac{\pi M_a(n) R_a^2(n)}{\Omega_a}\right)\nu_a(n)\right)\left(1 - 2\left(1 - \frac{\pi M_a(n) R_a^2(n)}{\Omega_a}\right)\nu_a(n)\right)\right]} \right. \\
&\left. \times \delta_{ij}\delta_{kl} + \frac{\left(\delta_{ik}\delta_{jl} + \delta_{il}\delta_{jk}\right)}{2\left(1 + \left(1 - \frac{\pi M_a(n) R_a^2(n)}{\Omega_a}\right)\nu_a(n)\right)} \right\}
\end{aligned}
\tag{5.37}
$$

The use of more advanced deterministic theories is known from the literature. However equivalent stochastic models are not available now. Similarly to a solid model with deterministic and stochastic microvoids, the stiffness reduction approach for cracked media can be applied as well [267]. The following material data are adopted for n=0: Young modulus E_m=2.1 E11, Poisson ratio ν_m=0.3, expected value of microvoids radius $E[r]$=0.1 and standard deviation of microvoids radius $\sigma(r)$=0.01, expected value of microvoids total number E[M]=1 and variance of microvoids total number Var(M)=0. The Young modulus is taken with ±10% deviations from the mean value the microvoid ratio variability is included in the interval [0,1.0]. Therefore an adequate visualisation of the component $C^{(eff)}_{1111}$ can be obtained, cf. Figure 5.4.

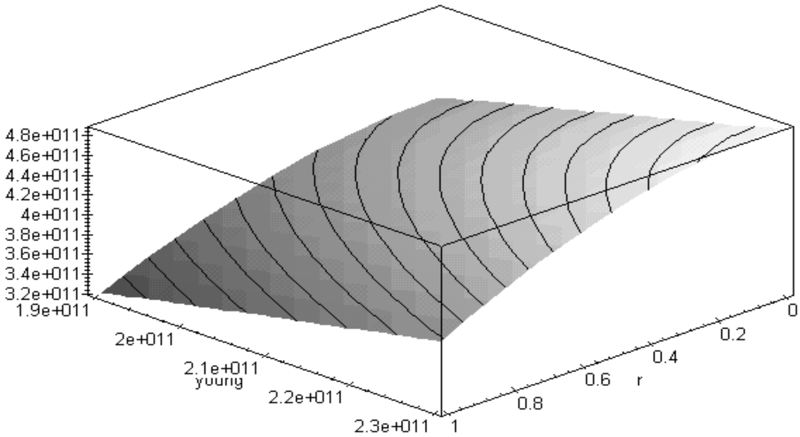

Figure 5.4. Parameter variability of $C_{1111}^{(eff)}$ for damaged homogeneous solid

Analysing the effective tensor surface, the expected linear dependence of this tensor on the Young modulus is observed as well as the nonlinear dependence on the microvoid mean radius (greater sensitivity to geometrical parameters of the structural defects). If only the statistical information about the input parameters is available, then the elasticity tensor can be rewritten using its first two probabilistic moments and introduced directly in SFEM analysis. If stochastic analysis in the elastoplastic range is necessary, the corresponding extension of the models presented in [355] can be applied. The microvoid volumetric ratio parameter is to be replaced with the two−parameter approach shown above and the probabilistic moments of these parameters are to be inserted as a function of the fatigue cycle.

As was mentioned before, the main goal of the homogenisation procedure is to find effective material properties of the homogeneous material, equivalent to the original composite. The most simplified method is to use the spatial average as the homogenised property and it is still used in terms of effective mass density, which can be rewritten for the nth cycle of fatigue analysis as

$$\rho^{(eff)}(n) = \left\langle \rho(n) \right\rangle_{\Omega} \tag{5.38}$$

Analogous homogenisation rule is applied in the case of heat capacity in transient heat transfer analysis and related thermoelastic or thermoelastoplastic coupled analyses of composites. The homogenisation of the elasticity tensor components is definitely more complicated and is usually carried out as

$$C_{ijkl}^{(eff)}(n) = \left\langle C_{ijkl}^{(a)}(n) \right\rangle_{\Omega} + \left\langle \sigma_{ij}\left(\chi_{kl}(n)\right) \right\rangle_{\Omega}, \quad \text{for } i,j,k,l=1,2,3 \tag{5.39}$$

where $\chi_{kl}(n)$ are the homogenisation function depending on the fatigue cycle.

The entire procedure can be applied for the fatigue analysis by rewriting the material properties of the composite components in terms of the current fatigue cycle number. Then, homogenising the constitutive law for each cycle, the whole composite fatigue can be modelled in a global scale, without the necessity for a very precise microscale discretisation or computational substructuring; an analogous analysis can be carried out for composite materials with cracks [336,337], for instance. It should be underlined that the described homogenisation procedure is sensitive to the RVE determination from the entire composite and to the scale parameter relating this element, dimensions to the dimensions of the entire composite. The formula for effective elasticity tensor is rewritten under the assumption that this parameter tends to 0, which is a very unrealistic model.

Furthermore, the homogenisation procedure can be established for random composites, too, only if the randomness does not influence the periodic character of the composite (especially during the fatigue process). Then, either MCS [191] as well as SFEM [192] can be utilised for this purpose. Therefore, starting from probabilistic characteristics of the composite properties, the expected values, variances (or standard deviations) as well as higher order moments (in the statistical estimation only) can be computed.

A very important issue from the technological point of view is the presence of the interface defects (usually with stochastic nature) appearing and growing between the composite components. Various computational models are proposed in this case in terms of special purpose spring finite elements or, alternatively, using the interphase as a new, separate material between the original composite components. This new material can be constructed from the original semicircular defects with random parameters, smeared (averaged probabilistically) over the entire interphase region according to the stochastic model introduced in Chapter 2; the composite with such an introduced interphase is then homogenised. To utilise the model for fatigue life cycle analysis, the geometrical and physical properties of the composite should be described in terms of the fatigue cycle number and then homogenised cycle by cycle for the needs of computational simulation of the composite.

5.3.1 Delamination of Two-Component Curved Laminates

Let us consider a two–component elastic transversely isotropic material in two–dimensional space Ω defined by the polar coordinate system $y=\{R,\Theta\}$ (cf. Figures 5.40–5.43). It is necessary to introduce the following relations:
(a) the gap between two surfaces

$$g(R,\Theta)=u_R^{(2)}(R,\Theta)-u_R^{(1)}(R,\Theta) \tag{5.40}$$

(b) the relative tangential slip of two surfaces

$$s(R,\Theta)=u_\Theta^{(2)}(R,\Theta)-u_\Theta^{(1)}(R,\Theta) \tag{5.41}$$

(c) the normal traction

$$\sigma_R(R,\Theta)=\sigma_R^{(2)}(R,\Theta)-\sigma_R^{(1)}(R,\Theta) \tag{5.42}$$

(d) the shear traction

$$\sigma_{R\Theta}(R,\Theta)=\sigma_{R\Theta}^{(2)}(R,\Theta)-\sigma_{R\Theta}^{(1)}(R,\Theta),\quad \Gamma_c=\left\{\Gamma_c : R=R_0;\Theta\in\left\langle 0,\infty\right\rangle\right\} \tag{5.43}$$

where R_0 is the radius of the interface curvature. Since (5.40) – (5.43) are referred to the composite interface (cracked or joined) Γ_c ($R=R_0=$const) only, then their radial dependence is neglected. The equilibrium problem of linear elasticity is given by the following equations system [95]:

- equilibrium equations

$$\frac{\partial\sigma_R}{\partial R}+\frac{1}{R}\frac{\partial\sigma_{R\Theta}}{\partial R}+\frac{1}{R}(\sigma_R-\sigma_\Theta)+b_R=0 \tag{5.44}$$

$$\frac{\partial\sigma_{\Theta R}}{\partial R}+\frac{1}{R}\frac{\partial\sigma_\Theta}{\partial\Theta}+\frac{2}{R}\sigma_{R\Theta}+b_\Theta=0 \tag{5.45}$$

where b_R and b_Θ denote the body force components;

- strain–displacement relations

$$\varepsilon_R=\frac{\partial u_R}{\partial R},\ \varepsilon_\Theta=\frac{1}{R}\frac{\partial u_\Theta}{\partial\Theta}+\frac{u_R}{R},\quad \varepsilon_{R\Theta}=\frac{1}{2}\left(\frac{1}{R}\frac{\partial u_R}{\partial\Theta}+\frac{\partial u_\Theta}{\partial R}-\frac{u_\Theta}{R}\right) \tag{5.46}$$

- constitutive relations

$$\begin{Bmatrix} \sigma_R \\ \sigma_\Theta \\ \sigma_{R\Theta} \end{Bmatrix} = \begin{bmatrix} C_{1111} & C_{1112} & C_{1113} \\ C_{2221} & C_{2222} & C_{2223} \\ C_{3331} & C_{3332} & C_{3333} \end{bmatrix} \begin{Bmatrix} \varepsilon_R \\ \varepsilon_\Theta \\ \varepsilon_{R\Theta} \end{Bmatrix} \tag{5.47}$$

The following boundary conditions are employed:

$$u_R = \hat{u}_R \quad \text{and} \quad u_\Theta = \hat{u}_\Theta \ \text{on} \ \Gamma_u \tag{5.48}$$

$$t_R = \hat{t}_R \quad \text{and} \quad t_\Theta = \hat{t}_\Theta \ \text{on} \ \Gamma_\sigma \tag{5.49}$$

$$g(\Theta) = 0\,;\ s(\Theta) = 0 \Rightarrow \sigma_R(\Theta) = 0\,;\ \sigma_{R\Theta}(\Theta) = 0 \ \text{on} \ \Gamma_c \tag{5.50}$$

$$g(\Theta) = 0\,;\ s(\Theta) \neq 0 \Rightarrow \sigma_R(\Theta) < 0\,;\ \left|\sigma_{R\Theta}(\Theta)\right| = \mu\left|\sigma_R(\Theta)\right| \ \text{on} \ \Gamma_c \tag{5.51}$$

$$g(\Theta) > 0\,;\ s(\Theta) = 0 \ \text{or} \ s(\Theta) \neq 0 \quad \sigma_R(\Theta) = 0\,,\ \sigma_{R\Theta}(\Theta) = 0 \ \text{on} \ \Gamma_c \tag{5.52}$$

$$g(\Theta) < 0\,;\ s(\Theta) \neq 0 \quad \sigma_R(\Theta) < 0\,;\ \left|\sigma_{R\Theta}(\Theta)\right| = \mu\left|\sigma_R(\Theta)\right| \ \text{on} \ \Gamma_c \tag{5.53}$$

$$sign\left(\sigma_R(\Theta)\right) = sign\left(s(\Theta)\right) \ \text{on} \ \Gamma_c \tag{5.54}$$

where μ denotes the constant friction coefficient. Then, the near−tip stress field is described in the polar coordinate system as $\{x\}=\{r,\theta\}$ (cf. Figure 5.6).

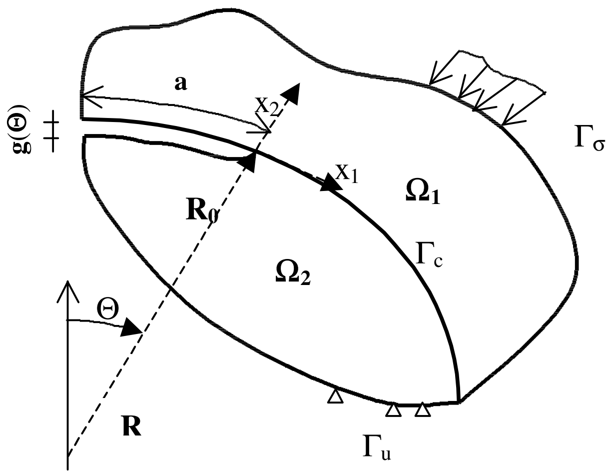

Figure 5.5. Two−component curved laminate structure

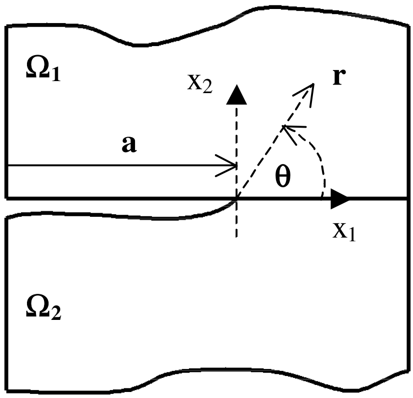

$x_1 = r\cos\theta$

$x_2 = r\sin\theta$

Figure 5.6. Near−tip field

It is assumed that both crack surfaces are modelled as perfectly smooth – there are no neither meso− nor micro−asperities on this surface in the context of the FEM contact model presented by [49,371,382], however application of the Boundary Element Method is also known, see [374]. Considering future particle-reinforced composites delamination simulations, the 3D contact algorithms must be employed [284,322]. The asymptotic nature of the elastic fields near a transition in the boundary conditions (crack tip) is expressed by the analytic functions and therefore, the description of a near−tip stress for an interface crack between two different transversely isotropic in a plane stress problem and the traction−free crack surfaces is given as follows [301]:

$$\sigma_{ij} = \mathrm{Re}\left[K\mathrm{r}^{i\in}\right](2\pi r)^{-0.5}\Sigma^{I}_{ij}(\theta,\in) + \mathrm{Im}\left[Kr^{i\in}\right](2\pi r)^{-0.5}\Sigma^{II}_{ij}(\theta,\in), \tag{5.55}$$

where i,j=1,2, $\Sigma^{I}_{ij}(\theta,\in)$, $\Sigma^{II}_{ij}(\theta,\in)$ are the angular functions derived using the Muskhelishvili potentials; $r^{i\in}$ describes here the oscillatory stress singularity given as

$$r^{i\in} = \cos(\in \ln r) + i\sin(\in \ln r) \tag{5.56}$$

The angular functions correspond to the normal and in−plane shear tractions, respectively, on interface ahead crack tip ($x_1>0$; θ=0) at a distance r given by [140,222]:

$$\begin{gathered}\sigma_{22} + i\sigma_{12} = K(2\pi r)^{-0.5} r^{i\in} \text{ or} \\ \sigma_{22} = \mathrm{Re}\left[Kr^{i\in}\right](2\pi r)^{-0.5} \text{ and } \sigma_{12} = \mathrm{Im}\left[Kr^{i\in}\right](2\pi r)^{-0.5}\end{gathered} \tag{5.57}$$

Moreover, the functions $\Sigma^{I}_{ij}(\theta,\in)$, $\Sigma^{II}_{ij}(\theta,\in)$ are related to the elastic properties of the bimaterial specimen using the oscillatory index $\in$ given by

$$\in = \frac{1}{2\pi} \ln\left(\frac{\kappa_1/G_1 + 1/G_2}{\kappa_2/G_2 + 1/G_1} \right) \tag{5.58}$$

where the Kolosov constant κ_n is given as [158,259]

$$\kappa_n = \frac{3-\nu_n}{1+\nu_n} \text{ for the plane stress} \tag{5.59}$$

$$\kappa_n = 3-4\nu_n \text{ for the plane strain; } n=1,2. \tag{5.60}$$

where ν_n and G_n denote the Poisson ratio and shear modulus of the nth component, respectively. Next, the elastic Dundur mismatch parameters are defined by

$$\alpha = \frac{G_1(\kappa_2+1) - G_2(\kappa_1+1)}{G_1(\kappa_2+1) + G_2(\kappa_1+1)} \quad \text{and} \quad \beta = \frac{G_1(\kappa_2-1) - G_2(\kappa_1-1)}{G_1(\kappa_2+1) + G_2(\kappa_1+1)} \tag{5.61}$$

Then, it is possible to rewrite (5.58) in the following way:

$$\in = \frac{1}{2\pi} \ln\left(\frac{1-\beta}{1+\beta} \right) \tag{5.62}$$

The fracture modes I and II [54] of the SIF in the case of an interface crack between dissimilar isotropic materials are now coupled together into the single complex SIF $K=K_1+iK_2$ uniquely characterising the singular stress field; K_1 and K_2 are the functions of a distance r from the tip and may be denoted as follows:

$$K_1(r) = \mathrm{Re}\left(Kr^{i\in}\right) \text{ and } K_2(r) = \mathrm{Im}\left(Kr^{i\in}\right) \tag{5.63}$$

The associated relative crack surfaces displacements ($\Delta u_i=u_i(r,\theta=\pi)-u_i(r,\theta=-\pi)$) at a distance r behind the tip ($x_1<0$; $\theta=\pm\pi$) are described in the following way:

$$\Delta u_1 + i\Delta u_2 = \left(\frac{1-\nu_1}{G_1} + \frac{1-\nu_2}{G_2} \right) \frac{Kr^{i\in}}{(1+2i\in)\cosh(\pi\in)} \left(\frac{r}{2\pi} \right)^{-0.5} \tag{5.64}$$

Finally, the ERR for the crack propagation along the interface may be given as

$$ERR = \left(\frac{1-\nu_1}{G_1} + \frac{1-\nu_2}{G_2} \right) \frac{K\overline{K}}{4\cosh^2(\pi\in)}, \tag{5.65}$$

where $\overline{K}=K_1-iK_2$ is the conjugate complex SIF. It finally gives

$$ERR = \left(\frac{1-\nu_1}{G_1} + \frac{1-\nu_2}{G_2} \right) \frac{\left(K_1(r)\right)^2 + \left(K_2(r)\right)^2}{4\cosh^2(\pi \in)}, \tag{5.66}$$

which makes it possible to calculate the material interface toughness starting from the local stress field under critical load.

The main goal of the computational experiments is to simulate the delamination process of a two−component layered composite subjected to shear loading in the shear device. It is predicted that near tip behaviour and frictional stresses along the crack surfaces are the main parameters governing the ERR. Therefore, the FEM−based numerical modelling of the delamination process is applied to get the accurate information about the following data: near−tip displacement and stress field description, normal stress distribution along the crack surfaces as well as the relation between the ERR and interface crack length.

A two−component curved composite beam is analysed numerically under the following assumptions: (i) the interlaminar adhesive layer has zero thickness (no contribution to ERR), (ii) near−tip stress field is analysed in the same way as the straight crack, (iii) the crack propagates along the interface only (kinking of a crack out of the interface is not considered), (iv) kinematic friction along the crack surfaces is accounted for, (v) friction between supporting jigs and the specimen is neglected (liquid lubrication of the tested material surface is assumed). The material components are homogeneous isotropic and linear elastic (cf. Table 5.1); geometrical data are given in Table 5.2 and Figure 5.7.

A FEM geometrical model is made from the three types of finite elements: 8−node plane stress quadrilateral with out−of−plane thickness (5.0e-3 m) and 4 integration points PLANE82 (structural solid), 3−node contact surface element with 2 integration points CONTA172 and 3−node target surface elements TARGE169. The last two element types simulate two essentially different kinds of material contact behaviour: flexible−to−flexible (between crack surfaces) and rigid–to−flexible (between the rigid curved device jigs and the curved specimen sides). For the present purposes, surface contact elements are more preferred than point−to−surface contact elements considering the curved geometry of a specimen and the requirements of a precise and detailed contact description as well as faster computational processing (smaller total number of contact finite elements). Moreover, target elements (CONTA172) simulating rigid curved jigs are modelled as longer than specimen curved sides (Θ_T+1°) to prevent loss of the contact at the model edges during the loading process. Crack tip vicinity is modelled by the ring of 16 8−noded finite elements (cf. Figure 5.9) introduced around 6−node triangular elements (PLANE82). The required square−root singularity on the element sides is achieved by the motion of the midside nodes of crack tip elements into the quarter points. Size of the crack tip element ring is 5.0 E-06 m in the radial direction, which corresponds to 0.02% of the component thickness (the characteristic length of a composite specimen). The very dense discretisation (cf. Figures 5.8 and 5.9) makes it possible to analyse the near−tip stress zone where the singular stresses dominate (in so−called K−dominance zone) with the length about 3% of the component thickness.

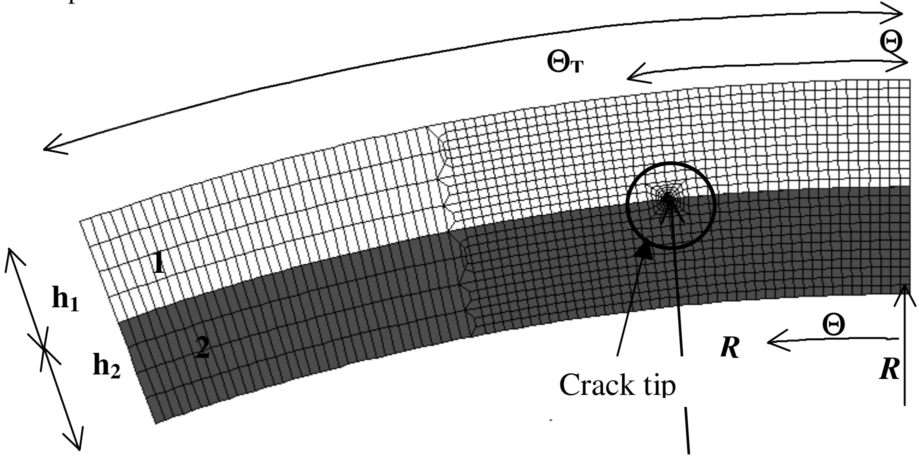

Figure 5.7. Composite beam geometry

Table 5.1. Material input data for FEM analysis

Material No.	Radial elastic modulus e_R [GPa]	Angular elastic modulus e_Θ [GPa]	Shear modulus $G_{R\Theta}$ [GPa]	Poisson ratio $\nu_{R\Theta}$
1	5.0	5.0	2.5	0.2
2	10.0	10.0	5	0.3

Table 5.2. Geometrical input data for FEM analysis

Component thickness [m]		Total angle Θ_T [deg]	Interface plane radius R_0 [m]	Crack propagation range Θ_a [deg]
h_1	h_2			
0.0025	0.0025	20	0.0525	<6-14>

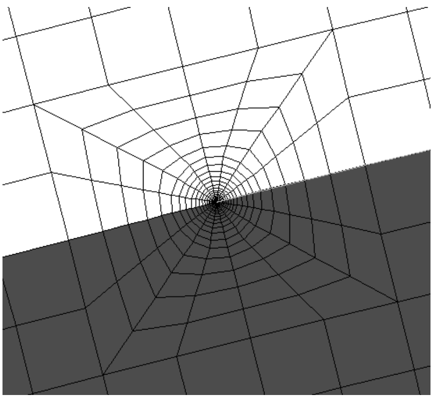

Figure 5.8. Crack tip zone discretisation

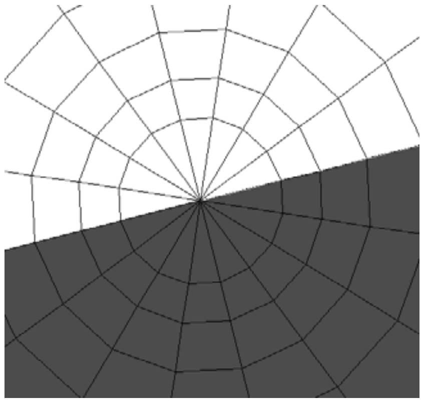

Figure 5.9. Crack tip mesh

The propagation of a crack is modelled computationally by the change of the crack tip position under constant radius value $R=R_0$. Thus, if the crack length increases during its propagation, the total number of elements and nodes increases as well as is comprised in the range between 2,302 and 2,878 finite elements (from 6,225 to 7,825 nodes).

The incremental nonlinear analyses (according to contact and friction) with two different boundary conditions (BC) and material configurations (cf. Table 5.3 and Figures 5.10 and 5.11) are performed to determine the influence of different load and material combinations on the contact between crack surfaces. The external loading is of static shear type and is applied in the form of displacement increments; the weaker component is loaded first.

Table 5.3. Geometrical boundary conditions for the composite beam

Case 1	Case 2
(i) $\Theta=\Theta_T$ and $R\in\langle R_0, R_0+h_1\rangle$: $u_R=0$ **(ii)** $\Theta\in\langle -1°, \Theta_T\rangle$, $R=R_0+h_1$: $u_R=u_\Theta=0$ **(iii)** $\Theta\in\langle 0°, \Theta_T+1°\rangle$, $R=R_0-h_2$: $u_R=0$; $u_\Theta=\tilde{u}$ **(iv)** $\Theta=0°$ and $R\in\langle R_0-h_2, R_0\rangle$: $u_\Theta=\tilde{u}$	**(i)** $\Theta=\Theta_T$ and $R\in\langle R_0-h_2, R_0\rangle$: $u_R=0$ **(ii)** $\Theta\in\langle -1°\ \Theta_T\rangle$, $R=R_0-h_2$: $u_R=u_\Theta=0$ **(iii)** $\Theta\in\langle 0°, \Theta_T+1°\rangle$, $R=R_0+h_1$: $u_R=0$; $u_\Theta=\tilde{u}$ **(iv)** $\Theta=0°$ and $R\in\langle R_0, R=R_0+h_1\rangle$: $u_\Theta=\tilde{u}$

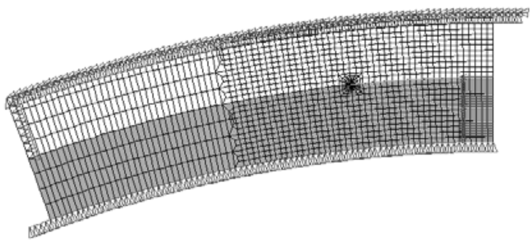

Figure 5.10. Model BC (case 1)

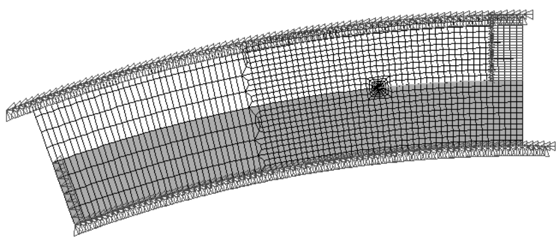

Figure 5.11. Model BC (case 2)

Frontal solver implemented of the ANSYS is used to solve the problem using the full Newton−Raphson iteration technique (stiffness matrix updated each time) together with the additional convergence enhancement tools: predictor−corrector and the line search options. The standard unilateral contact is modelled (pressure is equal to zero during separation) as well as one−pass contact (asymmetric contact) to obtain the equilibrium solution of contact tractions by means of the augmented Lagrangian method (iterative series of contact stiffness are updated for the contact stresses computation). Moreover, the unsymmetrical tangent stiffness matrix is used to derive of contact tractions what improved solution convergence in comparison with the symmetric tangent stiffness matrix approximation algorithm.

The cracks are closed on almost the entire length under applied shear loading, which results in sliding and sticking behaviour of the composite. Nevertheless, it is observed that in the case of weaker material loading, the area around the crack tip is opened which makes it possible to use the LEFM oscillatory theory of interfacial cracks in the ERR calculation. The length of the opened crack tip zones remains constant during crack propagation (about 1−2% of the total crack length, cf. Figure 5.12), while the crack opening maximum values are different for various crack lengths. It may be due to the change of the crack tip loading direction during crack propagation process. Moreover, the zero value of a crack opening shown in Figure 5.12 corresponds to sliding contact behaviour of the composite, which takes place in 98−99% of the crack length measured from the specimen edges; the asymptotic behaviour of stress is shown in Figure 5.13. The values of stresses depend asymptotically on the very high stress values up to values about 5 orders smaller and which are never equal to zero. Further, the oscillatory stress singularity is slightly influenced by the increasing friction coefficient μ and for extremal case (μ=1.0) the stress exponent is equal to λ=0.494.

Next, asymptotic behaviour of stress in the case of a completely closed crack (loading of stiffer component) is analysed in Figure 5.22. The extremal values of stresses (crack tip stress values) are considerably influenced by the friction coefficient increase and differ by about one order for μ=1. In this case the exponent λ depends on the friction coefficient μ and the interface fracture mechanics idea for the opened crack is no longer applicable. However, it is possible to calculate numerically the ERR for a closed crack with friction by means of the technique proposed in [292] using the FEM analysis [24], but here only the opened crack model is analysed. As can be expected, the stress tensor components around the crack for the test without the friction are essentially greater than those typical for the composite contact problem with a non−zero friction coefficient. It reflects the fact that some part of the internal strain energy is dissipated by the friction phenomenon in the second case, cf. Figures 5.14−5.21.

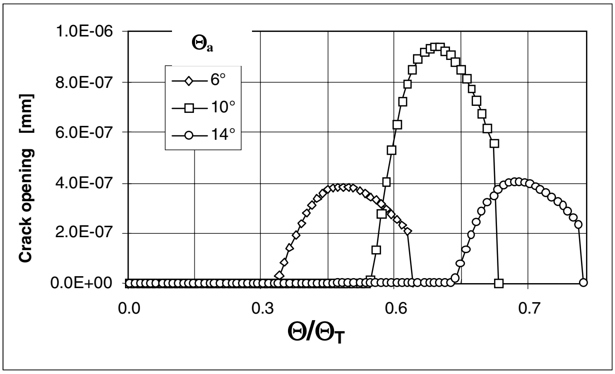

Figure 5.12. Crack opening displacement (case 1; μ=0.5)

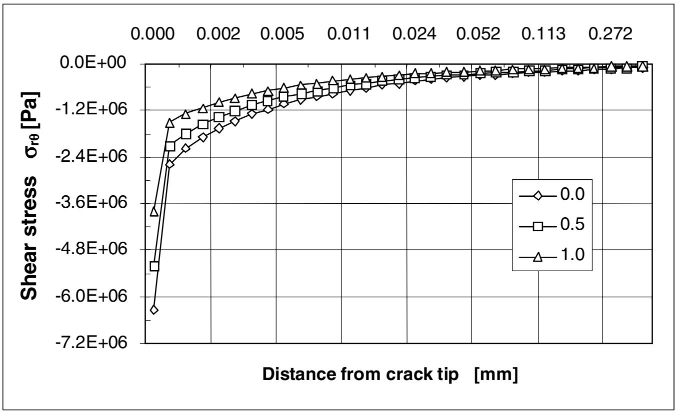

Figure 5.13. Near-tip stress dependence on μ (opened crack tip)

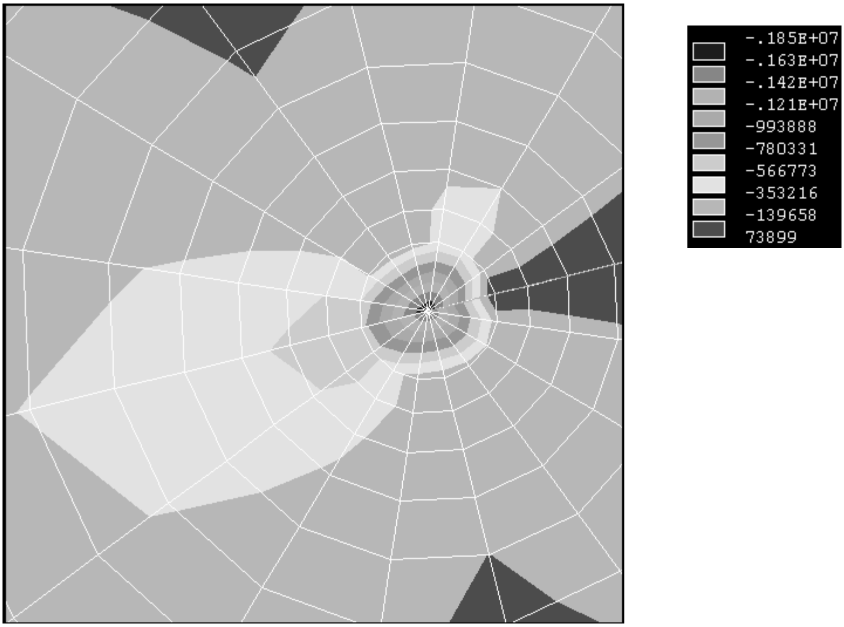

Figure 5.14. Near−tip stresses $\sigma_{r\theta}$ [Pa] (μ=0.5)

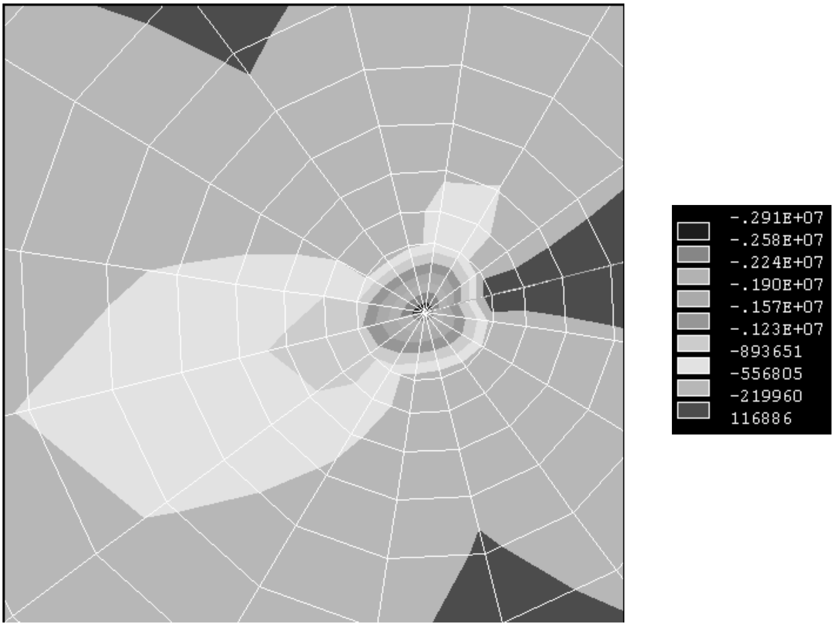

Figure 5.15. Near−tip stresses $\sigma_{r\theta}$ [Pa](μ=0)

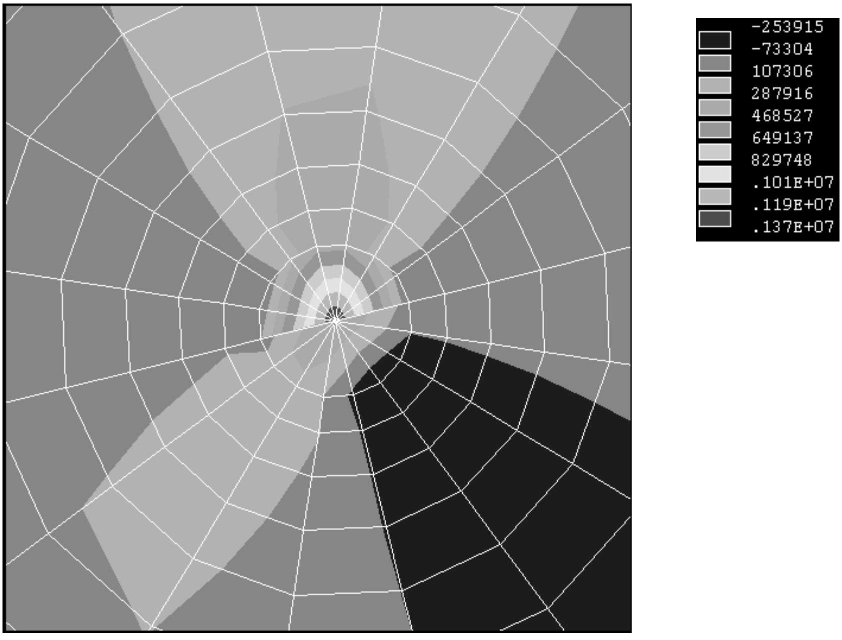

Figure 5.16. Near−tip stresses σ_r [Pa] (μ=0.5)

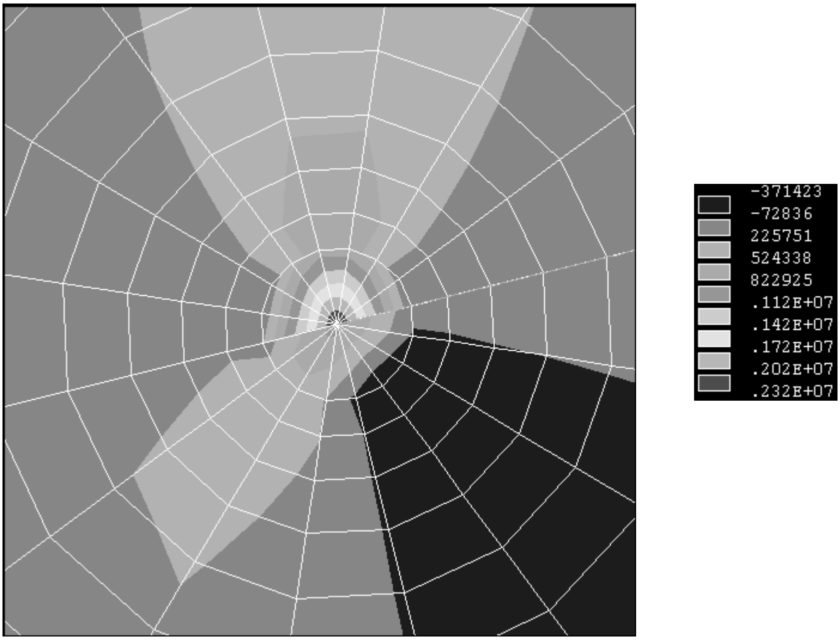

Figure 5.17. Near−tip stresses σ_r [Pa] (μ=0)

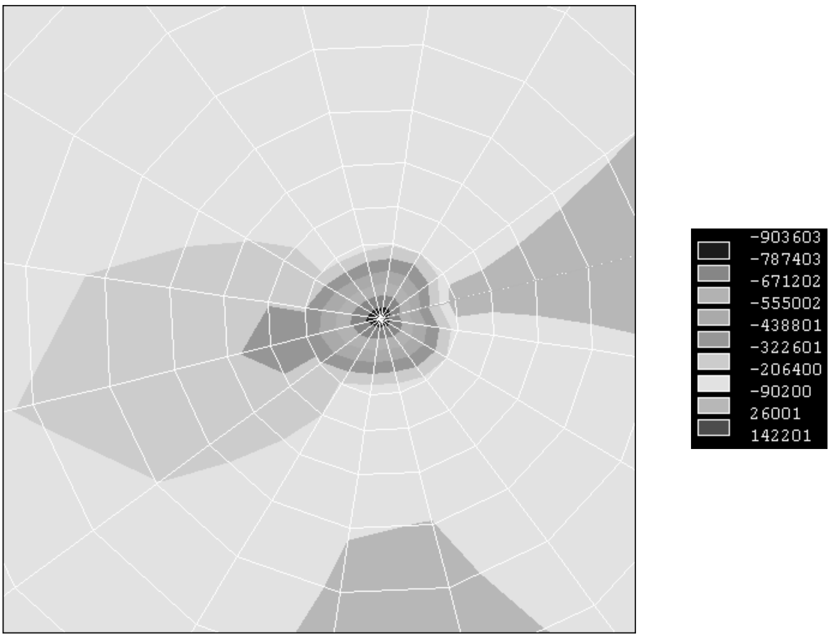

Figure 5.18. Near−tip stresses $\sigma_{r\theta}$ [Pa] (μ=0.5)

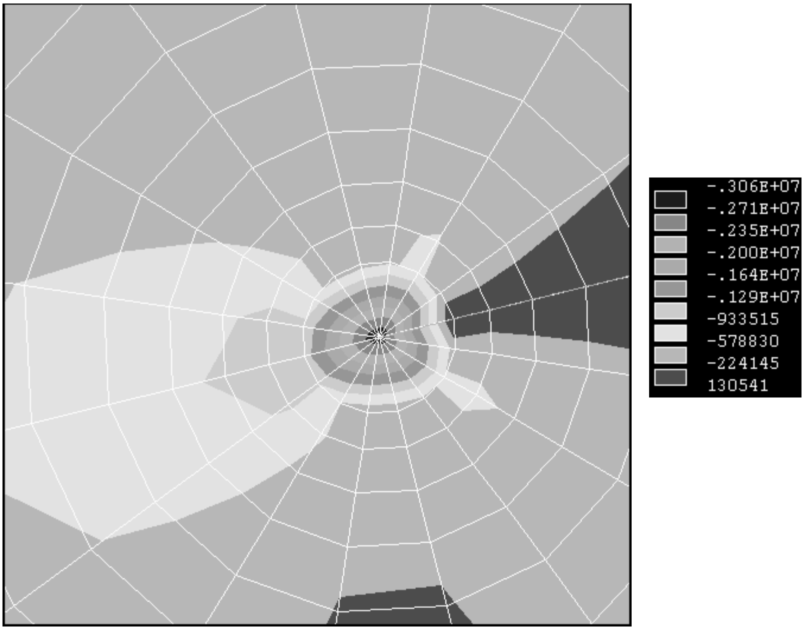

Figure 5.19. Near−tip stresses $\sigma_{r\theta}$ [Pa] (μ=0)

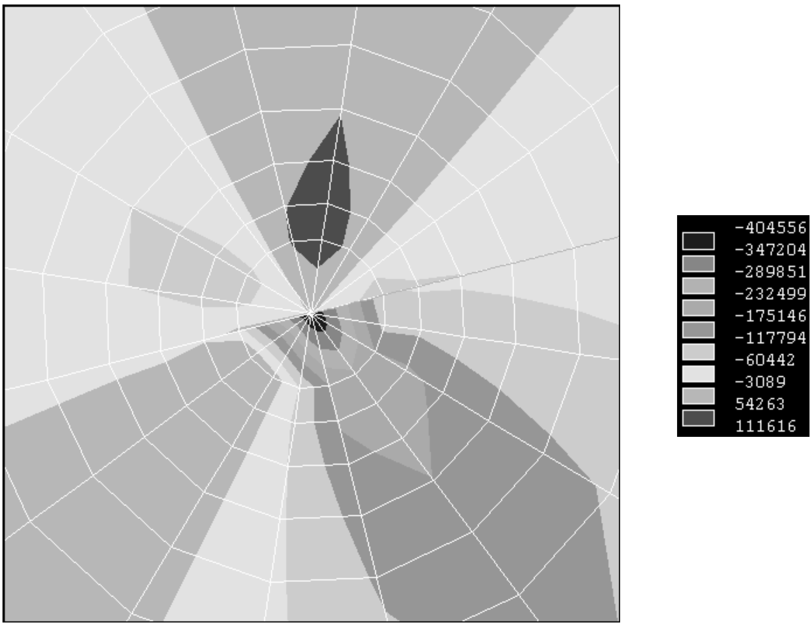

Figure 5.20. Near−tip stresses σ_r [Pa] (with μ=0.5)

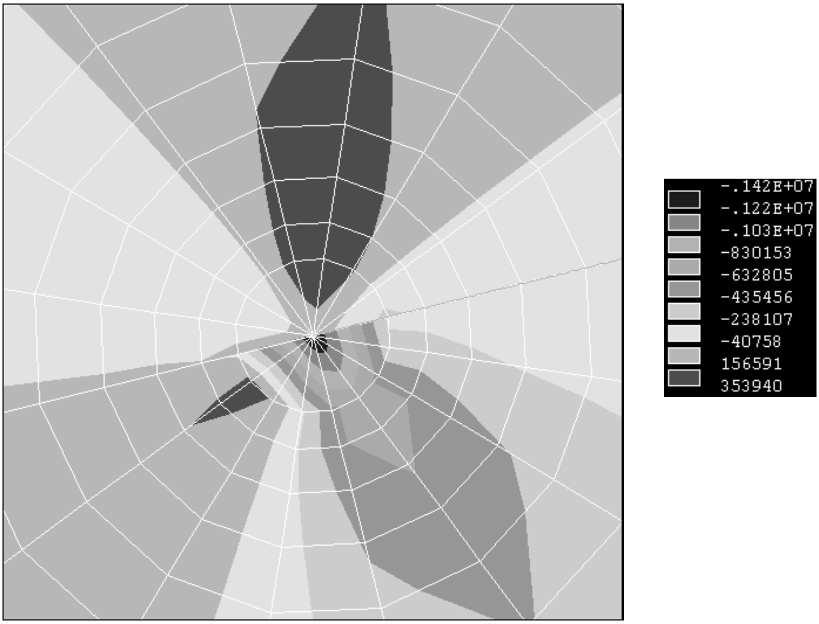

Figure 5.21. Near−tip stresses σ_r [Pa] (μ=0)

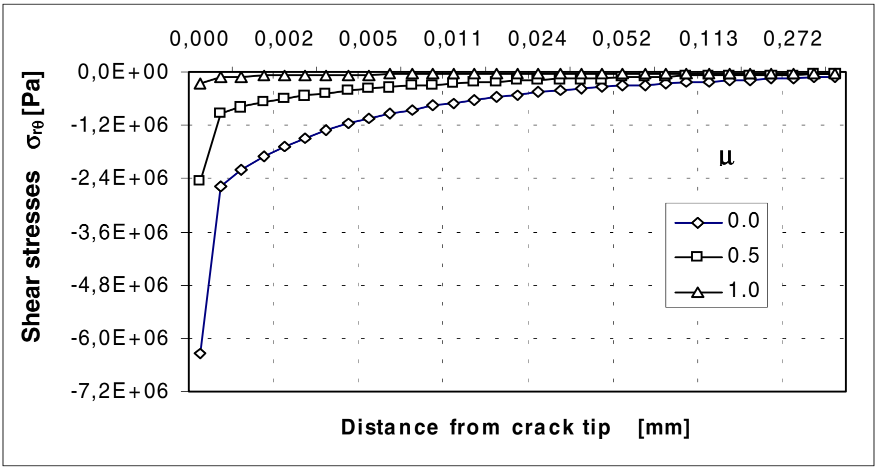

Figure 5.22. Near−tip stress dependence on μ (closed crack tip)

Further, normal stress distribution can be analysed along the crack length $\Theta \in \langle 0, \Theta_a \rangle$ (cf. Figures 5.23 and 5.24) from the model edge (zero crack length) to the crack tip for various crack lengths (Θ_a=6°, 10° and 14°). The uniform distribution of normal stresses σ_R, especially for longer cracks (Θ_a>9°), which is obtained in conjunction with constant value of μ, results in a uniform frictional stress σ_Θ along the crack surfaces according to Coulomb law. The part of the crack surface with quasi-uniform normal stress distribution increases together with the crack length increase as follows: 3.44E-3 m (6°), 7.33E-3m (10°), 8.93E-3 m (14°) for Figure 5.21 and 3.89E-3 m (6°), 5.04E-3m (10°), 8.93E-3 (14°) for Figure 6.22. It is reasonable because of the greater non-uniform deformation of the composite edges (due to BC) decreases with respect to the entire crack length during its propagation.

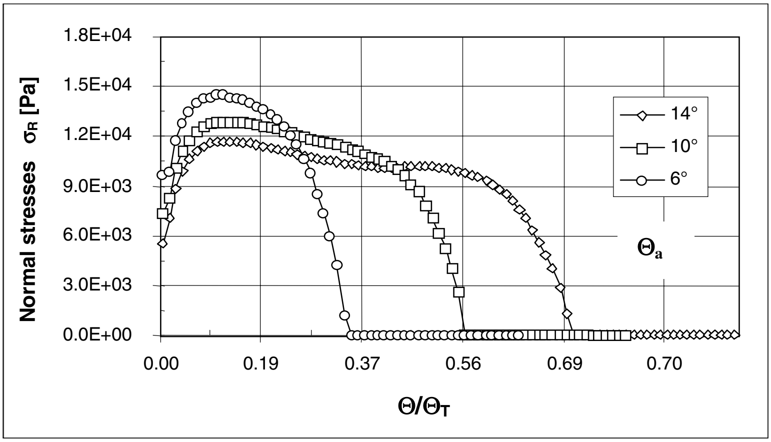

Figure 5.23. Normal stress distribution along the crack surface (case 1; μ=0.5)

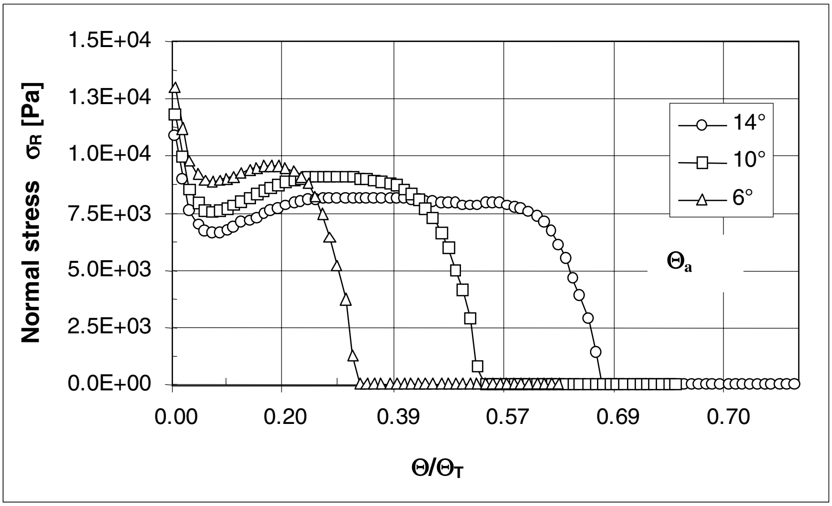

Figure 5.24. Normal stress distribution along the crack surface (case 2; μ=0.5)

The variable ERR is a function of the interface crack length and is computed for two different friction coefficients (μ=0 and μ=0.5). As is expected, a large decrease in ERR value follows the friction coefficient increase (cf. Figure 5.25).

For the shortest crack length (a_{min}=5.5E-3 m) the ERR takes value 1.54E-3 kJ/m^2 (μ=0) and 1.03E-3 kJ/m^2 (μ=0.5), while for the longest crack length (a_{max}=1.282E-2 m) the ERR value is equal to 8.71E-4 kJ/m^2 (μ=0) and 3.48E-4 kJ/m^2 (μ=0.5). Therefore, during the crack propagation from 5.5E-3 to 1.282E-2 m, the total amount of energy dissipated due to friction is comprised between 33 and 60% of the ERR value in the frictionless case. Moreover, the crack extension is stable (ERR decreases together with an increase of interface crack length), which means that a higher load should be applied to keep the growth of a crack. However, a friction phenomenon has a stabilising effect on the fracture process, which speeds up the ERR decrease together with crack length in comparison to a frictionless behaviour. Then, the quasi-stationary tendency of the ERR is observed for a certain crack length (a>1.1E-2 m) in frictional (from 3.9E-4 to 3.48E-4 kJ/m^2) and frictionless (from 9.06E-4 to 8.71E-4 kJ/m^2) cases. The stationary region of ERR may imply uniform crack tip load which would make it possible to determine experimentally the force responsible for delamination only; further analysis indicates the mode mixing of the fracture process. The shear mode prevails over the tensile mode of the ERR but the shear/tensile mode ratio (ERR2/ERR1) increases from 2.78 (a_{min}) to 2.88 (a_{max}) for μ=0 and decreases from 2.55 (a_{min}) to 2.45 (a_{max}) for μ=0.5. Although the friction influences both contributions of the ERR (ERR1 and ERR2), the ERR shear mode ERR2 is more reduced by the frictional stresses along the crack surfaces due to its direction during interface crack extension than the ERR tensile mode ERR1.

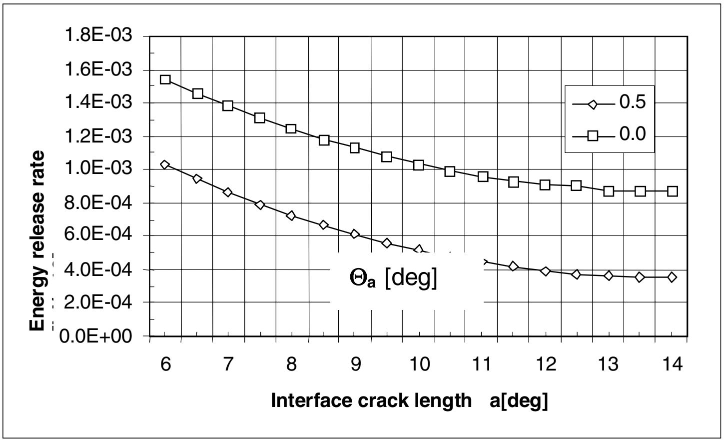

Figure 5.25. Energy release rate comparison

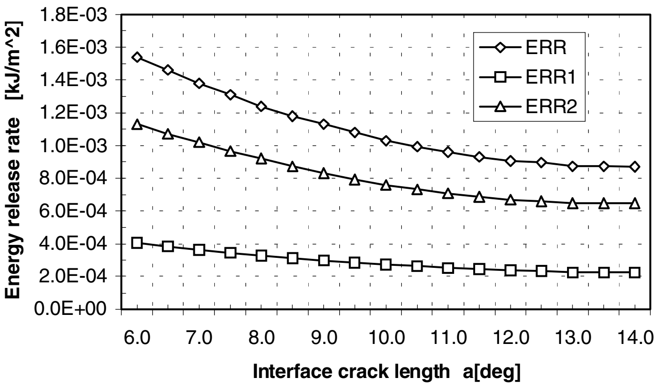

Figure 5.26. ERR contributions (μ=0)

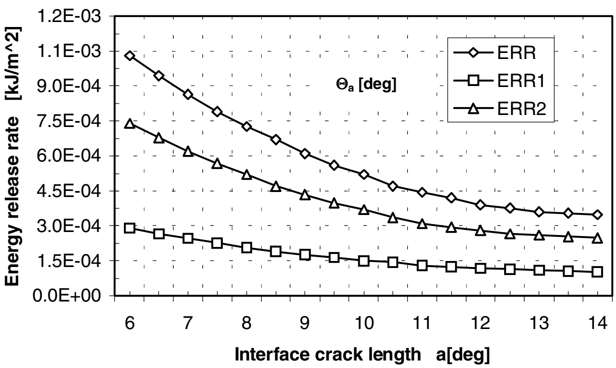

Figure 5.27. ERR contributions (μ=0.5)

The computations are performed on a single processor machine (700 MHz) with 256 MB (RAM) memory; the computer processing time (CP) and cumulative number of iterations (CNI) are presented in Table 5.4 as functions of various crack lengths for the 20th loadstep of the displacement increment.

Table 5.4. Computational experiments technical data

Crack length *a* [deg]	Element number	CP [s]		CNI	
		μ=0	μ=0.5	μ=0	μ=0.5
6	2302	12413.580	11809.241	292	263
10	2590	12958.353	15646.158	270	327
14	2878	10506.438	10735.686	230	231

It is observed that the CP time is not affected by the friction coefficient and the finite element number, but depends on some certain crack tip positions as the result of the curved model geometry. Thus, it is possible to point out that the critical crack length maximising CP and CNI exists and is equal to about Θ_a=10°.

5.3.2 Fatigue Analysis of a Composite Pipe Joint

A deterministic computational model of fatigue crack–like damage propagation in the composite pipe joint is introduced here and examined numerically using the FEM program ANSYS. The studies dealing with the other pressure vessels like longitudinally cracked pipes can be found in [142,218]. The model is built upon the following assumptions cf. [97,157,205,211,376]: (a) material components are linear elastic, (b) possible defect nucleation and growth is located within the adhesive layer and is caused by the high stress concentrations, (c) no initial manufacturing flaws, pre–cracks or other defects are assumed in the original adhesive layer (before the beginning of the fatigue loading process), (d) there are no microdefects forming and next coalescence during composite tension (typical for metallic materials) apart from crack formation and propagation, (e) the cyclic load has constant amplitude and (f) fatigue crack–like damage propagation is stable.

The stresses along the adhesive layer length are not uniform and their gradients arise at joint edges, which results from extension of the specimen layers in the opposite directions (composite pipe and coupling), cf. Figure 5.28. Then it is assumed that defects start to grow longitudinally along the adhesive layer and uniformly over all pipe circumference, under applied tensile load σ^{app}, when the resulting average shear stress $\langle\tau_{ad}\rangle$ over some distance d from the high stress concentration region is equal to or greater than the shear static strength τ_{ad}^{u} in adhesive layer. This criterion is expressed by the following equation:

$$\langle\tau_{ad}\rangle = \frac{1}{d}\int_0^d \tau_{ad}\, dX_A \geq \tau_{ad}^{u} \tag{5.69}$$

The formula (5.69) is called the average stress criterion after it was applied to notched strength prediction of laminated composites under uniaxial tension; a graphical representation of this criterion is shown schematically in Figure 5.28. The distance d is called the characteristic length and can stand for the damage accumulated or a nonlinear process zone. It is expressed here in terms of the critical fracture mechanics parameter as the critical Stress Intensity Factor (K_{IIc}) and shear strength of the adhesive layer as

$$d = \frac{1}{2\pi}\left(\frac{K_{IIc}}{\tau_{ad}^{u}}\right)^2 \tag{5.70}$$

Since (5.70) is based on the assumption of the square−root stress singularity in the front of the sharp crack tip, it does not precisely represent the stress distribution in the tubular adhesive layer in the stress concentration region. However, this characteristic length serves to estimate upper bound on the finite element size at the crack−like damage tip.

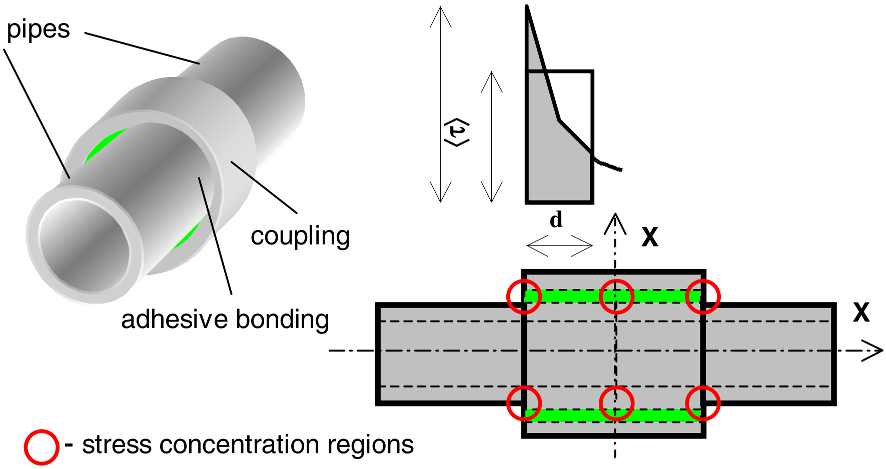

Figure 5.28. Pipe−to−pipe adhesive connection: 3D and 2D views

Then, it is postulated that after the crack−like defect had nucleated, it steadily propagates along the adhesive layer as the main single crack leading to an average stress increase over the distance d along with the number of load cycles N as

$$\langle \tau_{ad}(N) \rangle = \frac{1}{d}\int_0^d \tau_{ad}(N) dX_A \Rightarrow \frac{1}{d}\int_0^d \frac{\tau_{ad}(N)}{1-D(N)} dX_A \tag{5.71}$$

where $D(N)$ denotes the classical scalar damage variable, which may be written in terms of the nucleated and propagating main crack a as follows:

$$D(N) = \frac{a(N)}{l_a} \tag{5.72}$$

The defect propagation terminates according to the condition

$$D(N) = 1 \Leftrightarrow a(N) = l_a \tag{5.73}$$

which corresponds to the loss of stiffness for all those finite elements in the adhesive layer that are placed on the crack propagation path.

The boundary differential equation system, which describes fatigue defect propagation along the adhesive layer of a composite pipe joint may be defined over the pipe element of length $dl_a(N)=dX_A\text{-}da(N)$ as follows:
(i) equilibrium and damage equations

$$dF_p = dF_{ad}(N) \text{ and } dF_c = dF_{ad}(N) \tag{5.74}$$

$$d\sigma_p \frac{\pi}{4}\left(D_{op}^2 - D_{ip}^2\right) = \tau_{ad}(N)\pi\, D_{op} dl_a(N) \tag{5.75}$$

$$d\sigma_c \frac{\pi}{4}\left(D_{oc}^2 - D_{ic}^2\right) = \tau_{ad}(N)\pi\, D_{ic} dl_a(N) \tag{5.76}$$

(ii) constitutive relations

$$\frac{dw_p}{dl(N)} = \frac{\sigma_A}{E_p} \text{ and } \frac{dw_c}{dl(N)} = \frac{\sigma_A}{E_c} \tag{5.77}$$

$$\tau_{ad}(N) = \frac{G_{ad}\left(\gamma_p - \gamma_c\right)}{t_{ad}} \tag{5.78}$$

(iii) boundary conditions

$$\left.\frac{dw_p}{dl(N)}\right|_{X_A=L} = \frac{\sigma^{app}}{E_p} \text{ and } \left.\frac{dw_c}{dl(N)}\right|_{X_A=0} = \frac{\sigma^{app}}{E_c} \tag{5.79}$$

$$\left.\frac{dw_p}{dl(N)}\right|_{X_A=0} = 0 \text{ and } \left.\frac{dw_c}{dl(N)}\right|_{X_A=L} = 0 \tag{5.80}$$

where F_p, F_{ad}, F_c represent internal axial forces in a pipe, adhesive layer and coupling, respectively, internal axial stresses in the pipe, adhesive and coupling are denoted by σ_p, τ_{ad} and σ_c. Let us assume that E_p, E_c and G_{ad} are the axial modulus of the pipe, elastic modulus of the connecting layer and the adhesive shear modulus; w_p and w_c denote pipe and coupling axial displacements. This problem is now solved numerically for the pipe and coupling shear strains γ_p, γ_c and adhesive shear stresses $\tau_{ad}(N)$.

The main purpose of further computational studies is a prediction of crack damage propagation rate per a cycle in the composite pipe joint subjected to the pure tension fatigue load with the load time variations shown in Figure 5.29 (each load cycle is divided into two time intervals of 6 months). The cycle asymmetry ratio R is equal to 0, while the load amplitude is equal to the applied maximum load ($\sigma_{\max}^{app}$). Since quasistatic fatigue load is applied, no frequency effect is therefore considered here.

Let us note that the axis symmetry of the composite pipe joint results in simplification of the entire computational model and essentially speeds up the analysis process − only half of the composite pipe joint in the axial direction is considered only. The final computational model geometrical data to the FEM displacement−based commercial program ANSYS [2] are shown in Figure 5.30. The pipe and coupling component are made up of E−glass/epoxy composite (50% fibre volume fraction) and the adhesive layer (rubber toughened epoxy). All material properties of the composite pipe joint components are listed in Table 5.5.

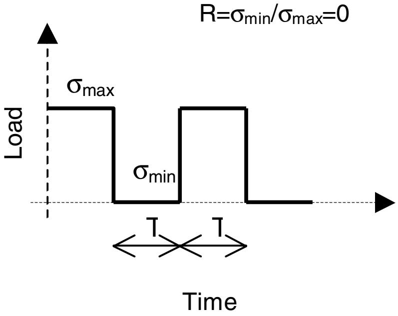

Figure 5.29. Applied fatigue load

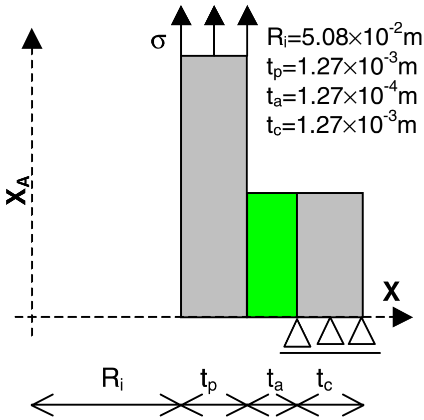

Figure 5.30. Computational model

The axisymmetric FEM analysis is carried out using four node finite elements PLANE42 of three translational degrees of freedom (DOF) (u,v,w) at each node. The model mesh is made to obtain greater density in high stress concentration regions (at both edges of the adhesive layer) − in this region the finite element size was equal to the process zone d given by (5.70). During loading process, the average value of the shear stress component computed by ANSYS in the finite element is compared to the static shear strength (σ_{ad}^{u}) of the adhesive layer. After this value had been exceeded within a finite element, then finite element stiffness was multiplied by the reduction factor equal to 1×10^{-6}, and the element was deactivated, until analysis was terminated.

Table 5.5. Material properties of the model

Property	Rubber toughened epoxy (joint)	E-glass/epoxy
Longitudinal modulus [GPa]	3.05	45
Transverse modulus [GPa]	3.05	12
Shear modulus [GPa]	1.13	5.5
Poisson ratio	0.35	0.28
Shear strength [MPa]	54	70
Tensile strength [MPa]	82	1020
Fracture toughness G_{Ic} [kJ/m^2]	3.4	-
Fracture toughness G_{IIc} [kJ/m^2]	3.55	-

Supposing that the shear mode of failure is dominating in the problem, several different failure modes may occur in composite pipe joints subjected to the tensile static load. That is why the distribution of stresses within the pipe, adhesive layer and coupling was analysed first to find out whether the shear stresses are the most decisive stress components for failure initiation within the adhesive joint or not. For the pipe joint geometry considered (cf. Figure 5.30), the computations predicted the bonding failure is dominated by the shear stresses, while other stress components (orthogonal and parallel) values were at least one order smaller. These results excluded other modes of failure for this specific model and load amplitude $\sigma_{\max}^{app}$ =270 MPa and, finally, confirmed appli cability of failure criterion (5.69).

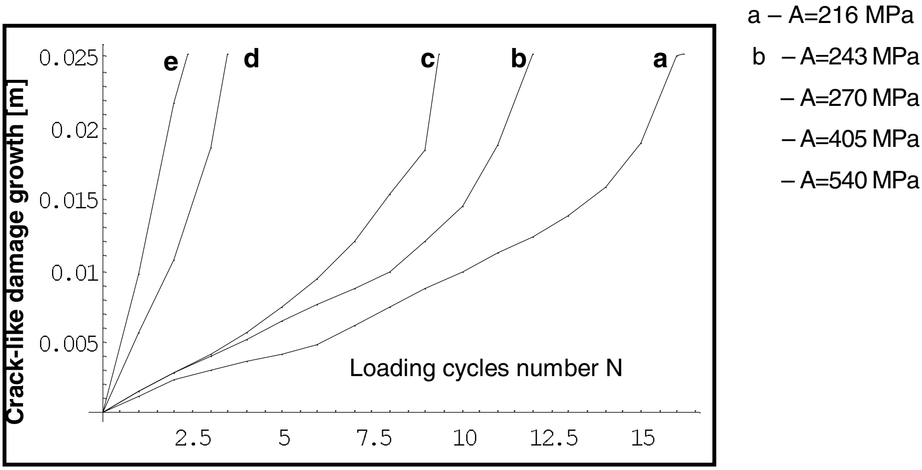

Figure 5.31. Crack−like damage growth under various amplitude fatigue loading

$$\sigma_m = 0.5(\sigma_{\max} + \sigma_{\min}) \text{ and } \left(\frac{da}{dN}\right)_m = \frac{1}{n}\sum_{i=1}^{n}\left(\frac{da}{dN}\right)_i \tag{5.81}$$

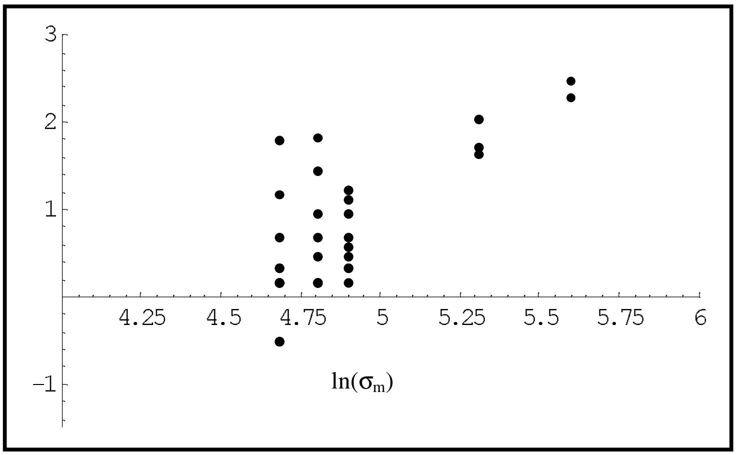

Figure 5.32. Crack-like damage growth per cycle

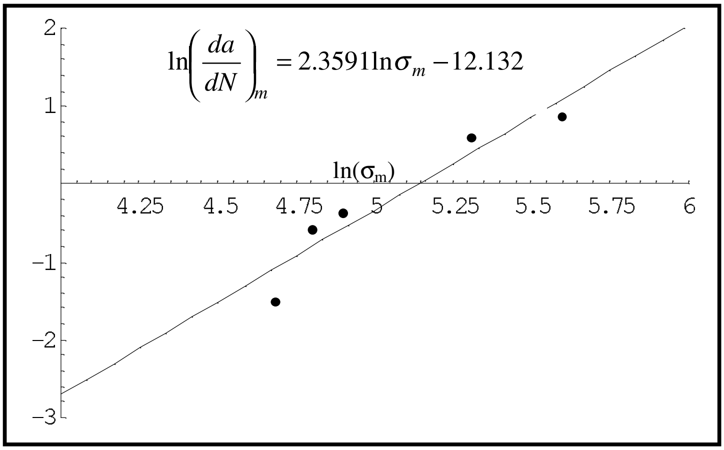

Figure 5.33. Fatigue constants estimation

The crack−like damage evolution in the adhesive layer is presented for five different load amplitudes $A=\sigma_{\max}^{app}$=216, 243, 270, 406 and 540 MPa as a function of load cycles. Those load amplitude values correspond to $4\times\tau_{ad}^{u}$, $4.5\times\tau_{ad}^{u}$, $5\times\tau_{ad}^{u}$, $7.5\times\tau_{ad}^{u}$ and $10\times\tau_{ad}^{u}$, respectively. They were chosen to find out the load amplitude effect on a composite pipe joint. Since below an applied load amplitude *A*=216 MPa no damage nucleation was observed, then this load value may be assigned to the load threshold, A_{th}. The tendency of longitudinal crack−like damage propagation was obtained from the computer analysis as the difference between crack−like damage tip at *N*th and (*N-1*)th cycle. The crack−like damage tip position was chosen to be the centroid of the finite element with reduced stiffness. Since the crack−like damage growth occurred from two opposite sides of the joint, thus two extreme longitudinal positions of the crack damage tips were considered and summed up to give a single crack−like damage value, as shown in Fig. 5.31. It is shown that an increase of amplitude resulted in a decrease of the load cycles were required for the final failure.

Then, the results from Figure 5.31 were used to calculate a mean crack−like damage propagation rate [mm/cycle] as a function of the applied mean fatigue−like load, calculated from (6.81) with the results shown in Figures 5.32 and 5.33.

A relation between the mean crack−like damage propagation rate and the applied mean stress is presented in Figure 5.33. The logarithmic form was taken in order to obtain coefficients α=2.3591 and β=-12.132 of the function $\ln(a)=\alpha\ln(b)+\beta$. The final relation between the mean crack damage propagation rate and the applied mean stress is given by the following equation:

$$\left(\frac{da}{dN}\right)_m = e^{\left[1\times10^{-4}\left(-121320.0+23591.0\ln\left(\sigma_m\right)\right)\right]} \tag{5.82}$$

The usage of (5.82) makes it possible to estimate the mean crack damage propagation rate under applied mean fatigue load, although it should be compared with other computational approaches to the problem or the relevant experimental results. For composite containing different material properties, it would be necessary to repeat all numerical procedures carried out here, because α, β are load− and material−dependent constants.

In order to present stress distribution during crack−like damage propagation, shear stresses are plotted for different load cycles in Figures 5.34−5.38. These stresses were determined as a function of the joint length in the middle of the adhesive layer thickness. The crack−like damage tips on both sides of a joint are denoted by 'A' and 'B'. It is shown that shear stresses at the crack−like damage tips increase along with load cycle number, as was expected. It is caused by the fact that the load transfer area from pipe to coupling decreases. The crack−like damage propagation is initially the same for both tips 'A' and 'B' and supported by similar shear stress magnitudes. Then, the shear stress magnitude changes and it is different at opposite crack damage tips. It probably results from the non−uniform extension of the crack damage across the remained adhesive layer. It is necessary to mention that the lower part of the pipe overlapped coupling before the failure, which does not demonstrate a realistic situation, where pipe and coupling would slide over each other.

The tendency of fatigue crack propagation was also inspected under different failure conditions utilising the concept of the average stress criterion. That is why the average orthogonal and parallel stresses were compared with relevant strength values for different amplitudes of the applied load. Computations revealed that it would be necessary to modify failure criterion, given by (5.69) to predict fatigue life as a combination of the average shear stress with average longitudinal tensile stress in case when applied load amplitude is higher than σ_{max}>406 MPa.

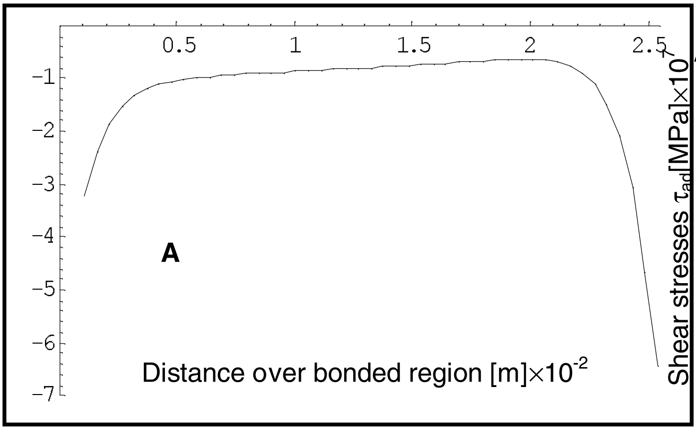

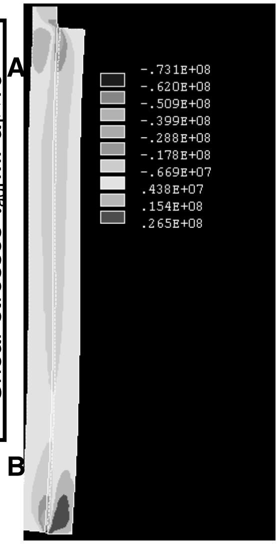

Figure 5.34. Shear stresses in undamaged adhesive layer

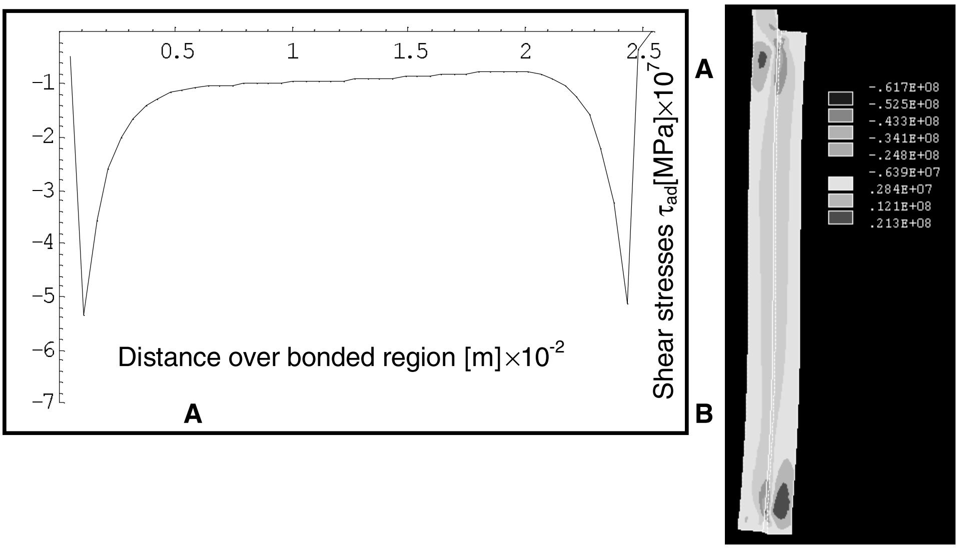

Figure 5.35. Shear stresses in adhesive layer after 1 cycle (1 year)

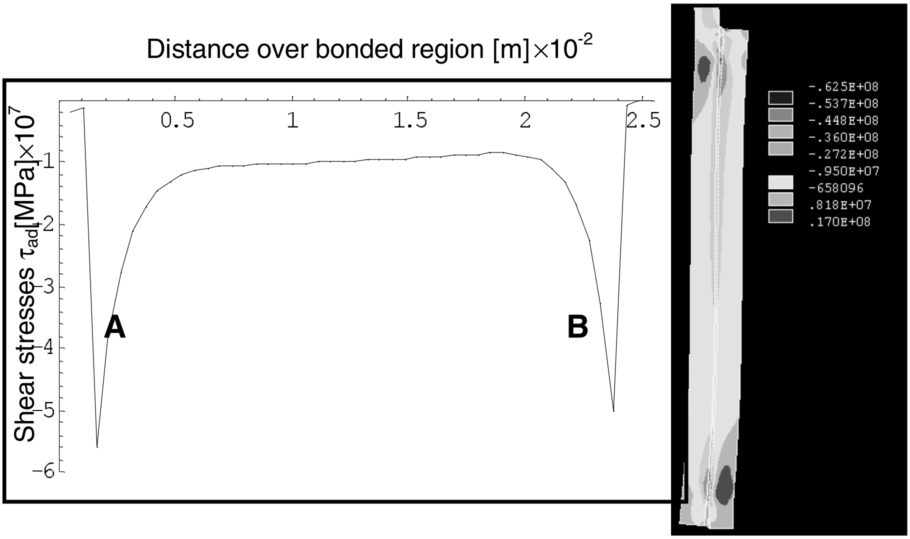

Figure 5.36. Shear stresses in adhesive layer after 2 cycles

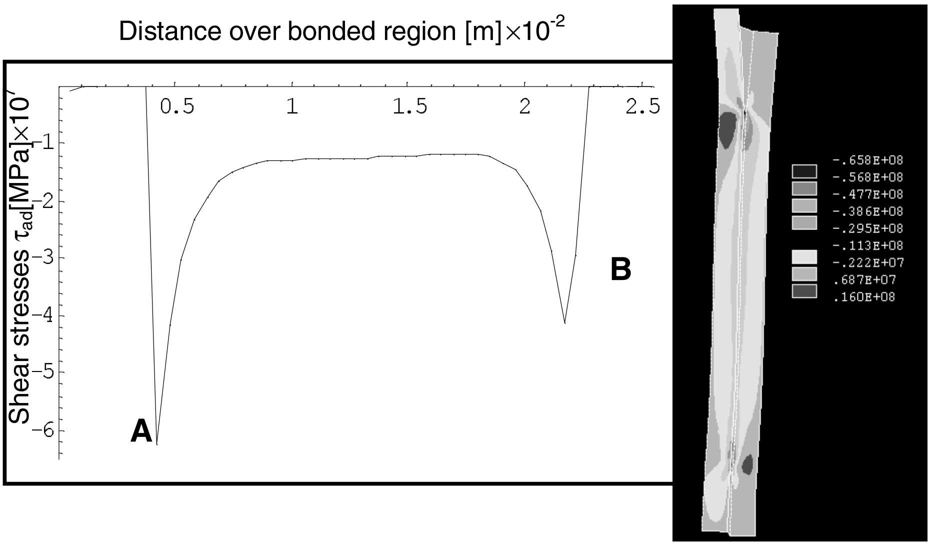

Figure 5.37. Shear stresses in adhesive layer after 5 cycles

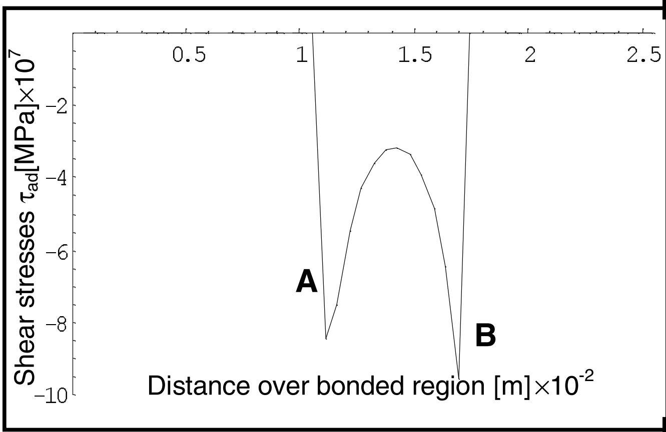

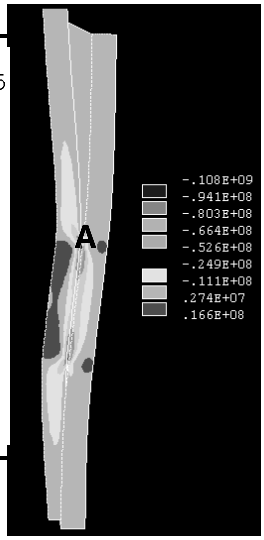

Figure 5.38. Shear stresses in adhesive layer after 9 cycles

Computations presented above are performed using 2,606 finite elements (254 in the adhesive layer); some numerical examples have been undertaken in order to estimate the total finite element number effect on the results. It was assumed that finite element number in the adhesive layer may only influence results by only. Thus the vertical mesh division effect was studied first with 400, 800, 1200, 1600, 2,000 and 4,000 finite elements, respectively. The results became independent from the decreasing finite element size (cf. Figure 5.39), while the critical finite element size for which results did not change was equal to $l_e \approx 0.0001$ m. It corresponds to about 250 vertical mesh divisions of the considered adhesive layer length.

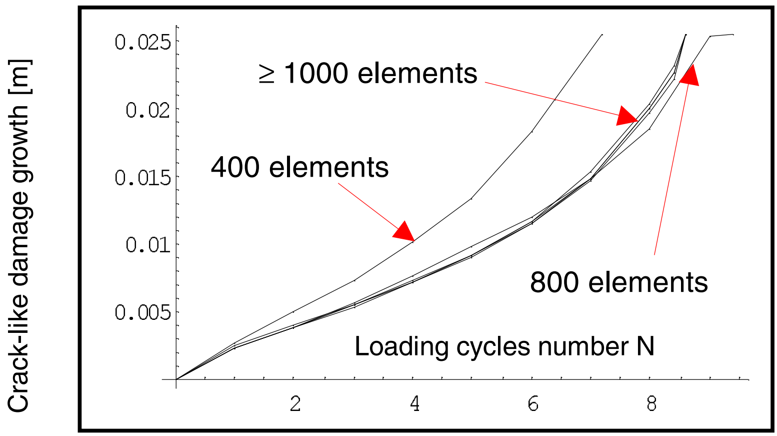

Figure 5.39. Fatigue life sensitivity to the finite elements number in adhesive layer

Numerical results presented in Figure 5.40 show that the finite element size simulating characteristic length d should be much smaller than those approximated by (5.70) and should be equal to $d \approx 0.0007$ m. Similar comparative study was carried out for different horizontal divisions and they demonstrated a rather small mesh effect on fatigue life prediction, which oscillated in that case between 8.4 and 8.6 load cycles number (cf. Figure 5.39).

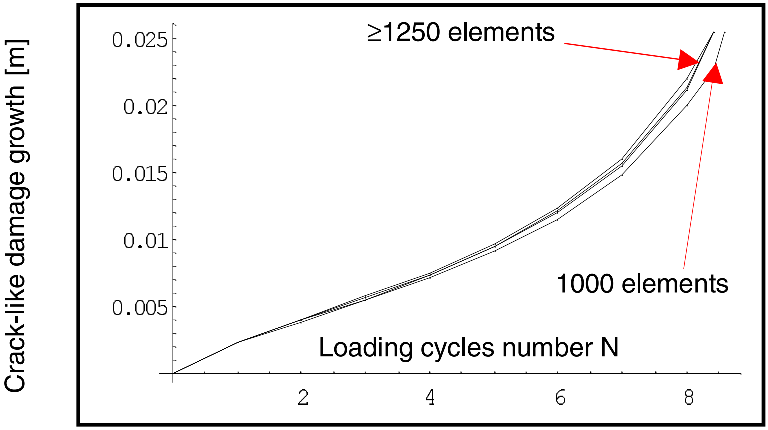

Figure 5.40. Fatigue life sensitivity to the finite elements number in adhesive layer

For the geometry of the model considered here, its finite element mesh of the adhesive layer should be designed using 5×250 elements (horizontal $\times$ vertical) in order to avoid a finite element mesh effect on the life prediction. Finally, it is suggested to solve numerically the problem by finite elements possessing a greater number of nodal degrees of freedom (nodal translations and rotations) such as shell finite elements, for instance, to improve the accuracy of the computational model.

The numerical approach proposed here enables efficient estimation of fatigue crack damage evolution rate in the composite pipe joint subjected to varying tensile load. This approach may be especially convenient in fatigue life prediction for the structures with high stress concentration regions, where internal stresses even under applied fatigue loading may be high enough to overcome material or component static strength. Qualitative numerical comparison of the fatigue crack damage evolution rate can be elaborated by the FEM displacement−based using cohesive zone fracture mechanics tools. In this case the damage of adhesive layer can be represented by a single crack model and crack evolution can be numerically determined e.g. through common spring finite elements, interface finite elements or solid finite elements with embedded discontinuity defined using the condition for a critical energy release rate growth.

5.3.3 Thermomechanical Fatigue of Curved Composite Beams

A two-component composite material with volume Ω is considered in the plane stress in an initially unstressed, undeformed and uncracked state, where its two constituents (Ω_1, Ω_2) are linear elastic and transversely isotropic materials; the effective elasticity tensor of the composite domain Ω is uniquely defined by their deterministic Young moduli and Poisson ratios. The problem is focused as before on the composite interface where a pre−crack of length a_o is introduced. Both crack surfaces are assumed to be perfectly smooth – there are neither meso− nor micro−asperities on their surfaces in the context of a contact model. The constant amplitude fatigue load σ_{ij} is applied with the coefficient of a cycle asymmetry $R = \sigma_{ij}^{min} / \sigma_{ij}^{max}$. The stress field under applied general transverse load at the crack tip is described by (5.57).

Now, let us analyse the fatigue phenomenon for such an interface [77,109,291,295], which results from thermo−mechanical external load cycles applied at the composite specimen [93,96]. Analogous to the classical Paris−Erdogan equation used to describe the fatigue crack growth rate in metals, its modified version is used

$$\frac{da}{dN} = c(\Delta G)^q \tag{5.83}$$

where c and q are some material constants determined experimentally. The energy release rate (ERR) range is described here as follows:

$$\Delta G = G^{\max} - G^{\min} \tag{5.84}$$

with $G^{\max}$ and $G^{\min}$ calculated for a certain applied load σ_{ij}^{max} and σ_{ij}^{min}, correspondingly. A quite similar fatigue analysis may also be applied in the case of thermal cycling or coupled thermomechanical fatigue analysis. However, it is necessary to apply the following equation to calculate the ERR range during periodic temperature variations:

$$\Delta G = G\left(T^{\min}\right) - G\left(T^{\max}\right) \tag{5.85}$$

where $T^{\min}$ and $T^{\max}$ are minimum and maximum temperatures for a given thermal cycle. The modified Paris−Erdogan equation (5.83) is used to estimate the number of fatigue cycles required for the steady state crack growth from an initial detectable precrack a_o to its critical length a_{cr}. It is assumed that once the critical crack length is reached, the crack grows continuously leading to the material failure by a delamination; this assumption determines the entire mechanism of a fatigue fracture of this particulate composite. Since that, the following fracture criterion is proposed:

$$\lim_{da\to 0}\frac{dG}{da}=\frac{G_{i+1}-G_i}{a_{i+1}-a_i}>0\Rightarrow a_{i+1}=a_{cr}\ \text{ and } G_{i+1}\geq 1.05G_i \tag{5.86}$$

The 5% factor is used in (5.86) to prevent instabilities of crack propagation and which is based on some computational observations presented later. On the other hand, if the ERR is less than the threshold value G_{th}, then no crack growth is observed.

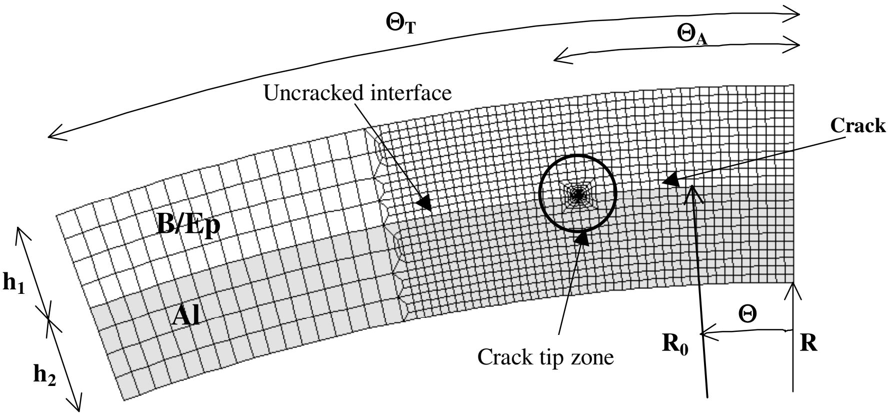

Figure 5.41. Composite FEM model

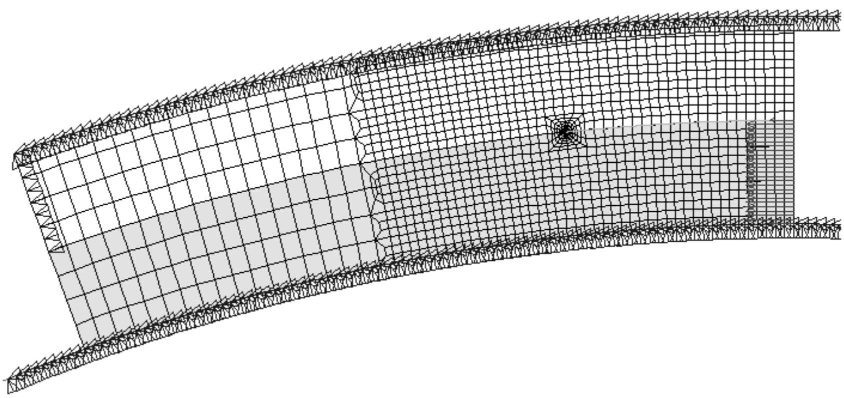

Figure 5.42. Mechanical boundary conditions

Moreover, it is possible to describe micro−crack density by the damage function as $D=a/a_{cr}$. In this case this function may be used to calculate the effective stress tensor for a cracked body as follows:

$$\sigma_{ij}^{eff(cr)} = \frac{\sigma_{ij}^{eff}}{1-D} = \frac{\sigma_{ij}(a_{cr}-a)}{a_{cr}} \tag{5.87}$$

where σ_{ij}^{eff} denotes the effective stress tensor of the initially perfectly bonded composite under applied load, which can be calculated by the classical homogenisation or mechanics of composite materials theory. Then, the effective stress tensor of a cracked body is estimated from (5.87) and is compared to the effective strength of a two−component curved composite.

The main purpose of computation is to estimate the number of load cycles required to composite fatigue failure by delamination as a function of the friction coefficient. The composite thermal cycling is simulated numerically to observe fatigue crack growth under non−mechanical loading. The analysis consists of the following steps in order to evaluate these parameters: (i) determination of the near-tip stress distribution under applied load (FEM analysis); (ii) evaluation of total ERR (and its contributions) as a function of the interface crack length and the friction coefficient; (iii) calculation of ERR range and (iv) determination of fatigue cycles to failure.

The composite FEM model for computer analysis is presented in Figures 5.41 and 5.42 − two linearly elastic transverse isotropic homogeneous components with the geometry parameters and material properties collected in Tables 5.6 and 5.7 are analysed.

Table 5.6. ANSYS geometrical input data

Component thickness [m]	h_1	0.0025
	h_2	0.0025
Total angle Θ_T [deg]; a_T [m]		20; 1.83×10^{-2}
Interface plane radius R_o [m]		5.25×10^{-2}
Pre-crack Θ_T [deg]; a_o [m]		6; 5.5×10^{-3}

Table 5.7. ANSYS input material properties

Property	**Boron/epoxy**	**Aluminium 7075-T6**
Density [kg/m^3]	2000	2810
Young modulus [GPa]	207	70.8
Poisson ratio	0.21	0.33
Shear modulus [GPa]	4.8	26.9
CTE [1/°C] $\times10^{-6}$	4.5	23.4
Conductivity [W/m°C]	14.7	130
Heat capacity [J/kg°C]	1150	960

The composite specimen is discretised in the FEM analysis using from 2,172 to 2,908 finite elements and from 5,863 to 7,879 nodal points to simulate the interface crack propagation. The crack length change is equal to 0.5deg (0.9×10^{-4}m). The very dense model discretisation around the crack tip needs a large effort for the singular near−tip stresses behaviour simulation. The elements used for model discretisation are 8−node plane stress solid elements PLANE82 (mechanical analysis) with 4 integration points and 8−node thermal solid elements PLANE77 (thermal analysis) with 9 integration points. Two−dimensional (2D) contact (CONTA171) and target (TARGE169) finite elements are used to simulate the contact with friction between crack surfaces and frictionless contact between external supports and model edges; the contact finite elements have 3 nodes and 2 integration points, while target finite elements are defined using 3 nodes. The numerical problem to be solved is geometrically nonlinear taking into account elastic contact with friction or frictionless elastic contact − that is why an incremental analysis is applied. The contact traction computation is possible thanks to the augmented Lagrangian technique with contact stiffness matrix symmetrisation. This technique as a combination of the two main constraint methods (penalty and Lagrange multiplier) is chosen in conjunction with predictor−corrector and the line−search numerical options to ensure satisfactory solution convergence.

The applied fatigue load is chosen as a compressive shear of 1.75 kN (138 MPa) with the cycle asymmetry factor R=0.017. It is observed that the shear contribution to the total ERR prevails ($\Delta G_2 \approx \Delta G_T$) over tensile mode under the given fatigue load. Since the shear mode dominates, the ERR is taken from the range $\Delta G = G_2^{\max} - G_2^{\min}$ only and its dependence on the friction coefficient is shown in Figure 5.43. The values of ERR range vary together with the coefficient of friction from 147 (a_o=5.49×10^{-3} m) to 183 J/m^2 (a_l=1.28×10^{-2} m) for μ=0 and from 108.4 (a_o) to 103.4 J/m^2 (a_l) for μ=0.15. The energy dissipated due to friction results in a reduction of the ERR and alters the tendency of crack propagation − it stabilises the fracture process.

That is why the critical crack lengths corresponding to the lowest values of friction coefficients are equal to a_{cr}=5.2 mm for μ=0.0 and μ=0.01, which are smaller than those obtained for μ>0.01 and equal to a_{cr}=7.4 mm. Thus, the number of cycles to composite failure by delamination is based on the critical crack length criterion and is calculated from (5.83). The parameter q=10 and the ERR threshold ΔG_{th}=100 J/m^2 are applied together with the parameter c=1×10^{-26}. The results of the composite life prediction are shown in Figure 5.44 – we observe there that the friction coefficient increases strongly and decreases the crack growth rate per cycle which finally leads to composite fatigue life improvement, under the assumption that interface delamination does not bring about other damage processes such as wear, for instance. Finally, the number of fatigue cycles to composite failure are estimated to be N_f=61,865 cycles for μ=0 and N_f=5.067040×10^6 cycles for μ=0.14.

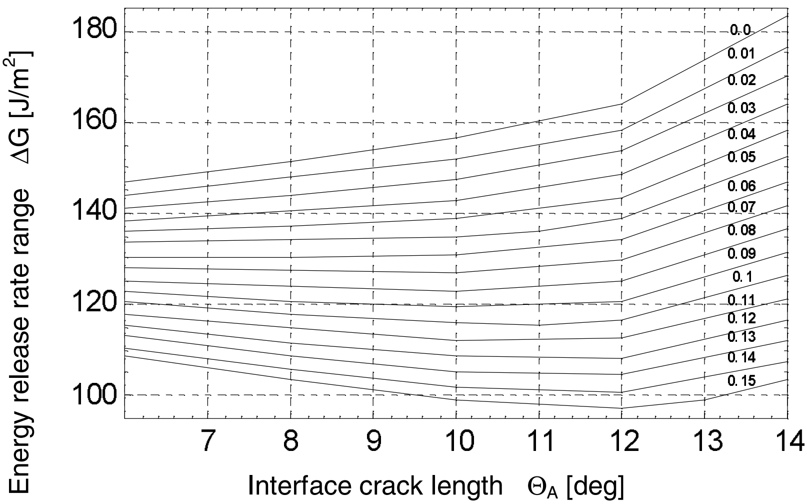

Figure 5.43. Energy release rate range during fatigue crack growth

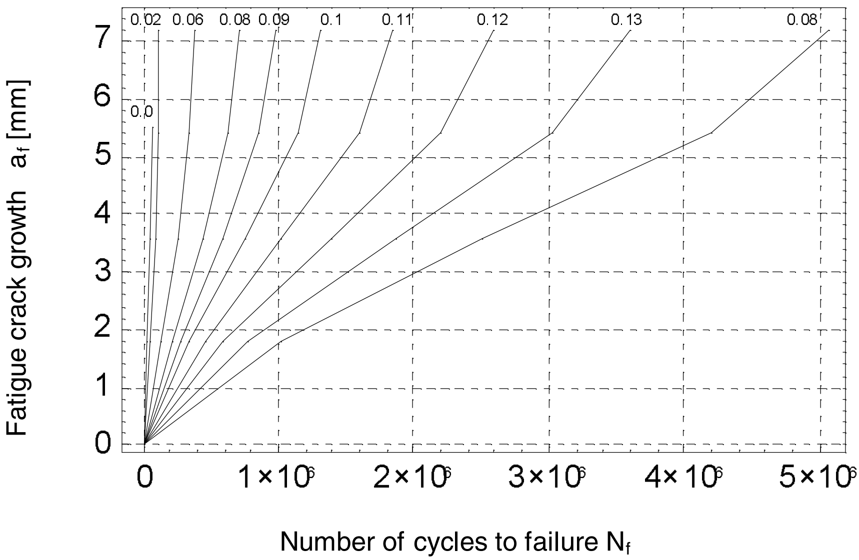

Figure 5.44. Composite mechanical fatigue life

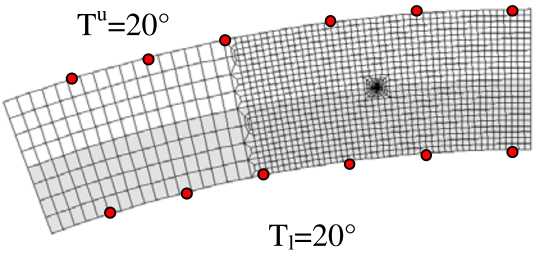

Figure 5.45. Initial temperature conditions

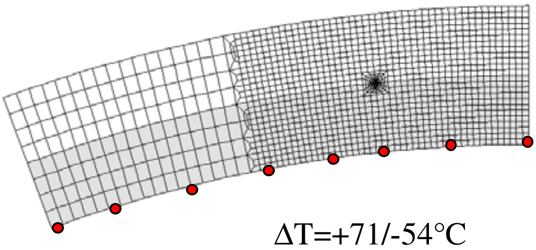

Figure 5.46. Thermal cycling

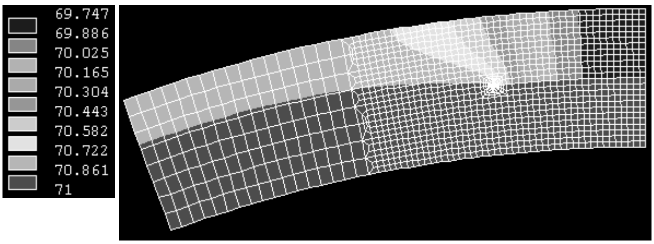

Figure 5.47. Temperature distribution (1st cycle, T=+71°C)

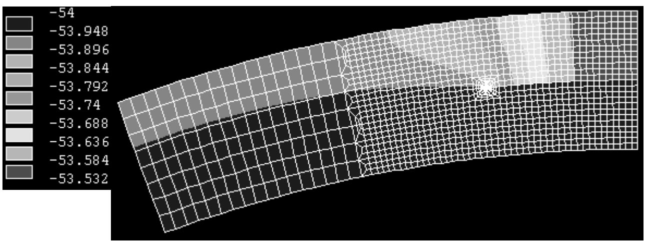

Figure 5.48. Temperature distribution (1st cycle, T=-54°C)

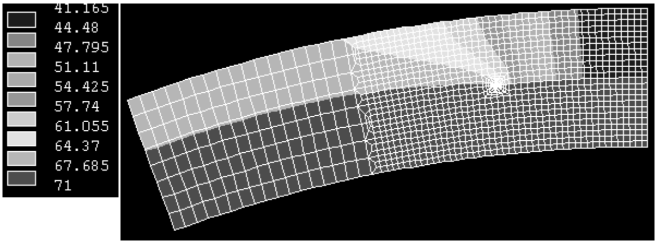

Figure 5.49. Temperature distribution (25th cycle, T=+71°C)

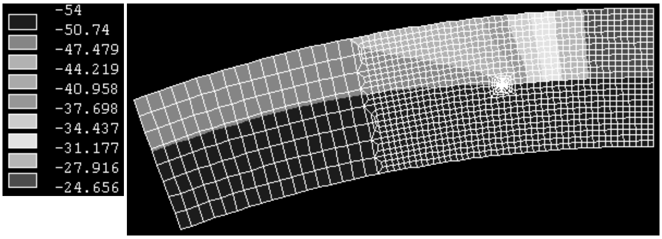

Figure 5.50. Temperature distribution (25th cycle, T=-54°C)

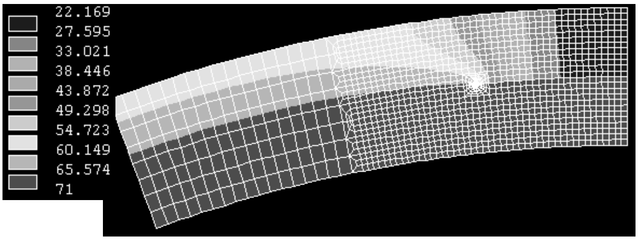

Figure 5.51. Temperature distribution (50th cycle, T=+71°C)

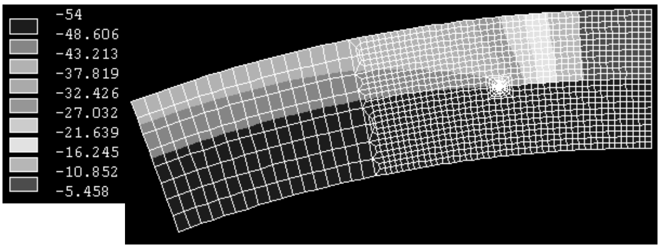

Figure 5.52. Temperature distribution (50th cycle, T=-54°C)

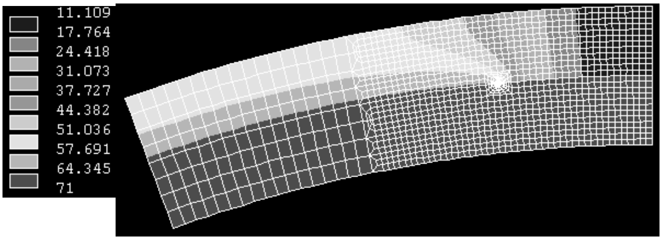

Figure 5.53. Temperature distribution (75th cycle, T=+71°C)

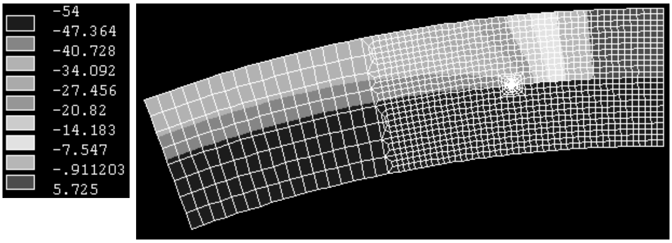

Figure 5.54. Temperature distribution (75th cycle, T=-54°C)

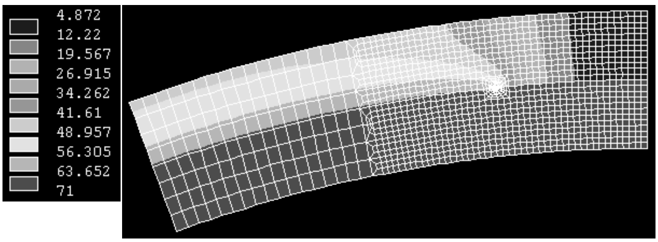

Figure 5.55. Temperature distribution (100th cycle, T=+71°C)

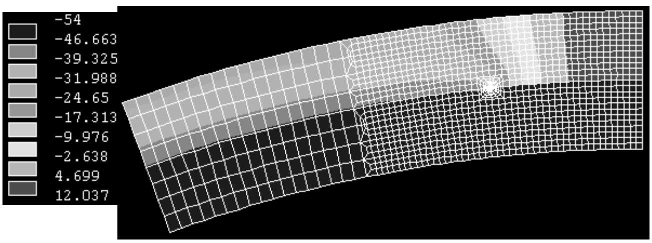

Figure 5.56. Temperature distribution (100th cycle, T=-54°C)

Computational thermal cycling is carried out for the composite specimen in the temperature range T^{max}=+71 and T^{min}=-54 – thermal boundary conditions are presented in Figures 5.44 and 5.45. First of all, the stationary thermal analysis is worked out to introduce the initial conditions for temperature distribution (cf.

Figure 5.44). Then, thermal cycling is carried out thanks to the non−stationary thermal analysis implemented in the program ANSYS. The number of simulated fatigue cycles is taken as 10 E5 cycles for +71/-54°C and corresponds to the total time t=252,000 s, where Δt=1260 s is used in numerical analysis as an incremental time step. As is shown later, the fatigue crack growth after 100 cycles is very small and equal to $\Delta a=3\times10^{-6}$ m. Therefore, the analysis is carried out for the initial crack length $a_o=5.5\times10^{-3}$ m. Initially, the temperature has almost the same value in all composite regions. Then, the difference in temperature increases together with the number of thermal cycles, and even temperatures with opposite signs are observed in opposite composite regions (upper and lower component). It is predicted that the near-tip stress range can be reduced if the temperatures of opposite signs appear on either side of the composite interface.

The temperature distribution over the laminate cross−section is presented for 25, 50, 75 and 100 cycles in Figures 5.49−5.56 for two temperatures mentioned above. Comparing Figures 5.47, 5.49, 5.51 and 5.53 illustrating the temperature distributions for greater initial temperature at the bottom of a laminate, it is seen that the minimal temperature is decreasing together with an increase of the fatigue cycle number (a composite is frozen during a fatigue analysis). Quite the opposite observation can be made for T=-54°C (cf. Figures 5.48, 5.50, 5.52, 5.54 and 5.56). The maximal temperature increases from T=-53.5°C (for 1st cycle) to about 12°C which means that the composite is heated during the delamination process. For both initial temperatures at the bottom of a structure, spatial distributions of temperature gradients are exactly the same.

The results of non−stationary analysis give an input for a mechanical analysis carried out for a composite model subjected to zero external mechanical loads. However, the composite is circumferentially fixed by the target finite elements and on the left side of the upper component by the supports. This coupling makes it possible to analyse the thermal stresses in a composite and further, to determine the ERR range. As was noticed before, the near−tip stress range is reduced during thermal cycling.

The equivalent thermal stresses $\sigma^{(th\text{-}eqv)}$ distributions around the crack tip are shown in Figures 5.57−5.62 for an initial crack length (a_o) at the upper and lower limit temperatures (+74°C and –54°C). Thermal stresses range is reduced from $\Delta\sigma^{(th\text{-}eqv)}$=-1000 MPa (after the 1st cycle) to -930 MPa (after 100 cycles).

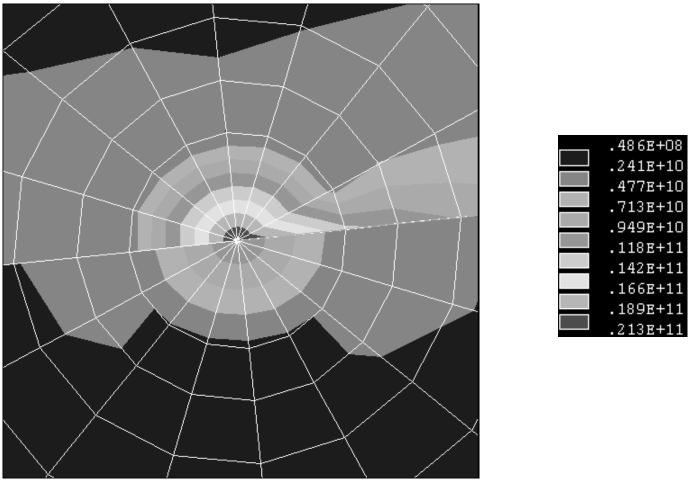

Figure 5.57. Thermal equivalent stress $\sigma^{(th\text{-}eqv)}$ [Pa] (1st cycle; +71°C)

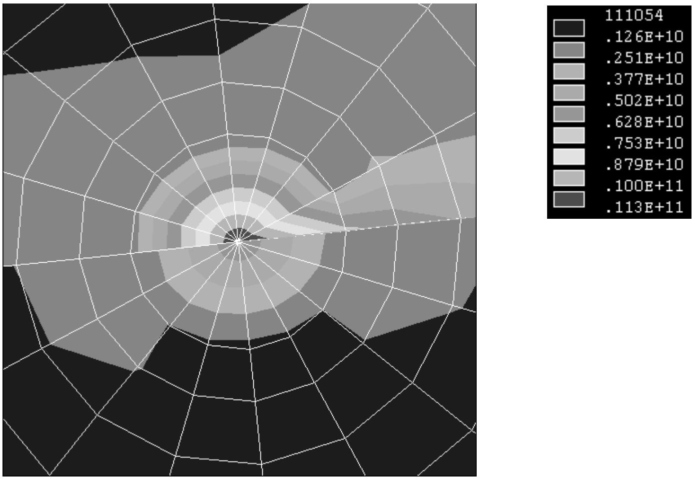

Figure 5.58. Thermal equivalent stress $\sigma^{(th\text{-}eqv)}$ [Pa] (1st cycle; -54°C)

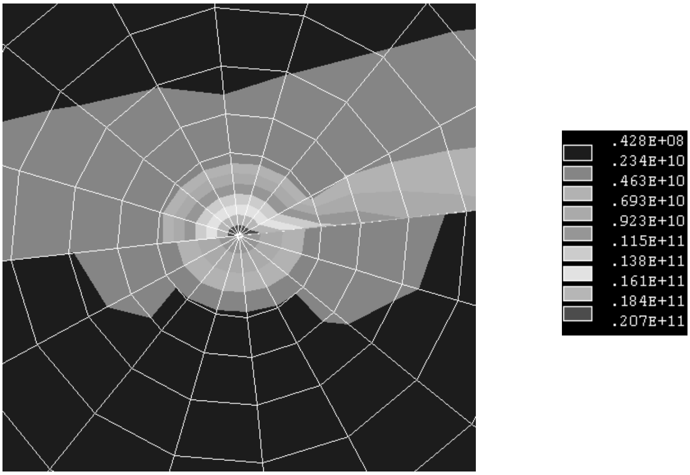

Figure 5.59. Thermal equivalent stress $\sigma^{(th\text{-}eqv)}$ [Pa] (50th cycle; +71°C)

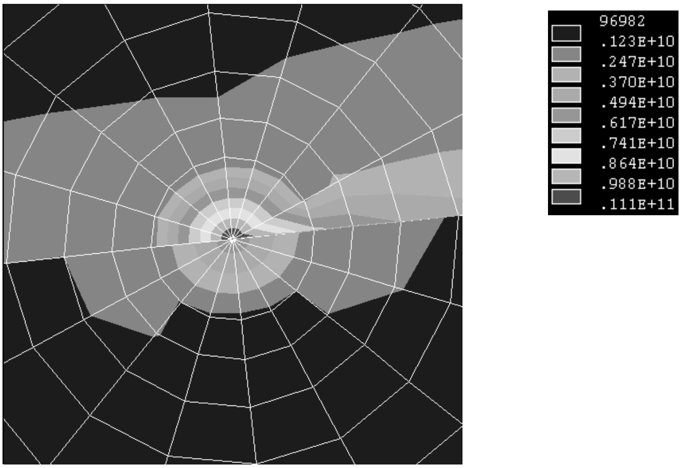

Figure 5.60. Thermal equivalent stress $\sigma^{(th\text{-}eqv)}$ [Pa] (50th cycle; -54°C)

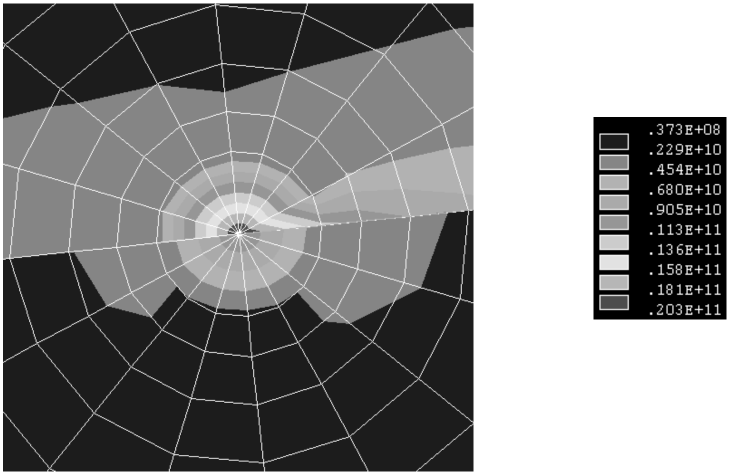

Figure 5.61. Thermal equivalent stress $\sigma^{(th\text{-}eqv)}$ [Pa] (100^{th} cycle; +71°C)

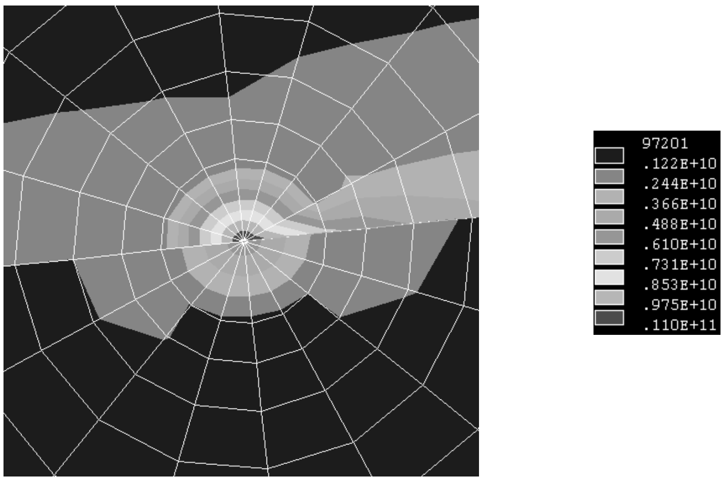

Figure 5.62. Thermal equivalent stress $\sigma^{(th\text{-}eqv)}$ [Pa] (100^{th} cycle; -54°C)

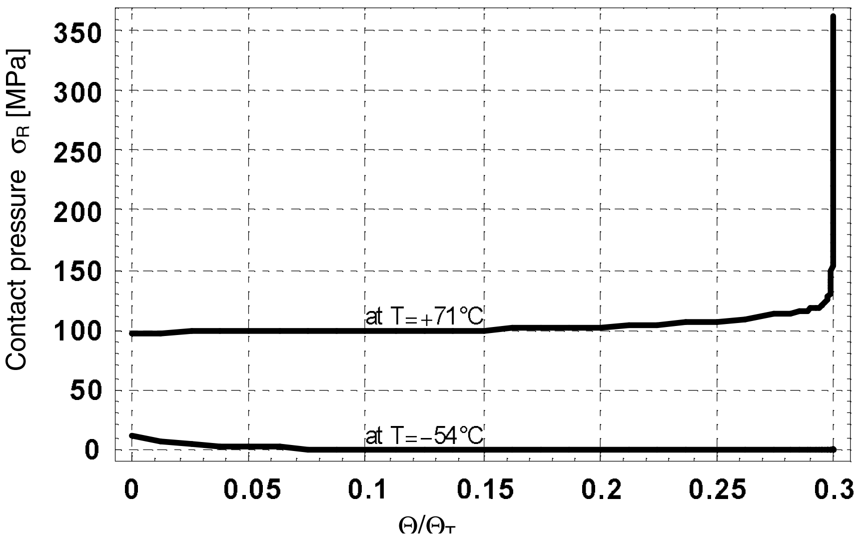

Figure 5.63. Contact pressure along the normalized crack length

Comparing these figures it can be noticed that thermal equivalent stresses are generally greater for greater initial temperature. Further, as can be expected, the maximum value of these stresses for both temperatures decreases together with an increase of the fatigue cycle number. Next, it is observed that material deformation at the upper temperature limit (+71°C) led to crack surface contact the over total crack length, while at the lower temperature limit (-54°C) the crack surfaces are opened along almost the entire crack length with the closed region near the specimen edge a_{cl}=1.14×10^{-3} m; it can be observed in Figure 5.63, where the contact pressure distribution along crack surfaces is presented after the 1st and 100th thermal cycle; a region characterised by the contact pressures σ_R=0 MPa corresponds to the crack opening. The normalised crack length equal to 0.3 is referred to the crack tip position, where the contact pressure at T=+74°C is reduced by about 10% after 100 thermal cycles.

The computed range of ERR is presented as a function of the interface crack length for a constant friction coefficient μ=0.0 in Figure 5.64. The total ERR range as a function of the interface crack length has a decreasing tendency. Mode I of the ERR range prevails, contrary to the ERR range contributions obtained from mechanical cycling, and is comprised of between 93.4% (a_o=5.4×10^{-3} m) and 95.2% (a=7.2×10^{-3} m) of a total ERR range, while the fatigue crack is arrested at a_{arr}=6.3×10^{-3} m according to the assumption of fatigue crack growth threshold ΔG_{th}=100 J/m^2.

Finally, the ERR range determination makes it possible to estimate the number of thermal cycles necessary to hold up the fatigue crack growth. The same fatigue constants as in the case mechanical fatigue are used to calculate the fatigue cycle number. The number of thermal cycles to increase the crack length from a_o to a_{rr} is equal to N_{arr}=1.012155×10^6 cycles (cf. Figure 5.65). As fatigue crack is arrested and supported by the decreasing ERR range (see Figure 5.64), no criterion of composite failure is possible to take into account the crack propagation instability. That is why it would be feasible to use (5.87) to estimate the fatigue damage accumulation influence on the overall composite properties, replacing a_{cr} by a_{arr}.

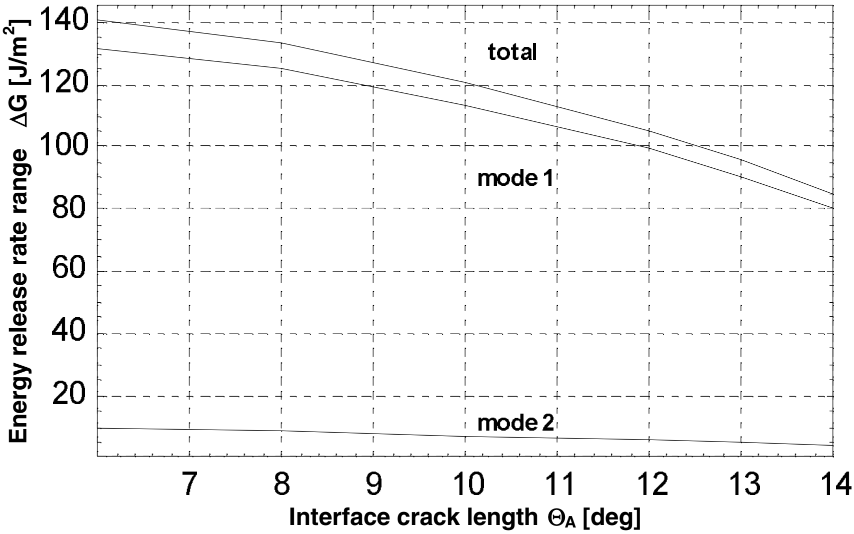

Figure 5.64. Energy release rate range

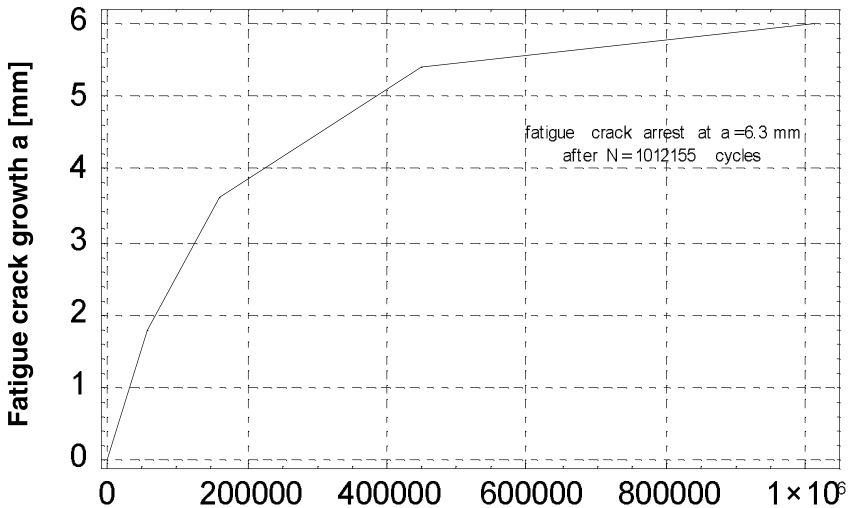

Figure 5.65. Number of cycles to fatigue crack arrest

5.4 Perturbation–based Fracture Criteria

Contrary to the traditional fracture criteria used in both deterministic analysis and stochastic Monte Carlo simulations, the probabilistic fracture criteria consist of probabilistic moments of material strength as well as the corresponding moments of external load and its direction angle. The second order perturbation technique is applied below to rewrite the Tsai–Hill criterion in terms of expected values and standard deviations of all quantities discussed.

It is expected that a failure criterion is a function of material strength and the stress (or strain) applied at the specimen. While for isotropic and homogeneous materials such a condition should not be relatively complicated, in the case of composites, the total strength is a function of composite type, the principal directions of the structure and the stress applied as well as the angle relating this stress to the direction introduced. One of the most popular in composite engineering are Tsai–Hill and Tsai–Wu failure criteria, which may be rewritten as follows:

$$\frac{\cos^4\theta}{X^2}+\left(\frac{1}{S^2}-\frac{1}{X^2}\right)\cos^2\theta\sin^2\theta+\frac{\sin^4\theta}{Y^2}=\frac{1}{\sigma^2} \tag{5.88}$$

X, Y, S denote composite strengths in the three principal directions (longitudinal, transverse and shear, respectively) while σ and θ denote externally applied axial stress and the angle between this stress and principal direction X [352];

$$\begin{gathered}\frac{cos^4\theta}{X_tX_c}-\frac{sin^2\theta cos^2\theta}{\sqrt{X_tX_cY_tY_c}}+\frac{sin^4\theta}{Y_tY_c}+\frac{sin^2\theta cos^2\theta}{S^2}\\+\left(\frac{1}{X_t}-\frac{1}{X_c}\right)cos^2\theta+\left(\frac{1}{X_t}-\frac{1}{X_c}\right)sin^2\theta=\frac{1}{\sigma^2}\end{gathered} \tag{5.89}$$

where X_t, X_c, Y_t, Y_c and S are axial strength in tension, compression and transverse strength in tension and compression as well as shear strength, as previously. Equations (5.88) and (5.89) can be rewritten for the needs of probabilistic analysis after some basic algebraic transformations, while all of the quantities appearing in these equations may be treated as random variables.

Let us consider a fracture criterion for a composite being a function of material properties and stress tensor components to introduce the perturbation–based fracture analysis

$$f(\sigma;\mathbf{X})=0 \tag{5.90}$$

In terms of random loads and/or probabilistically given composite properties it can be said that (6.90) is verified with probability almost equal to 1. Since the fact that the character of the final probability density function (PDF) is unknown then denoting by $\mu_k(f(\sigma,\mathbf{X}))$ the kth order probabilistic moment of the failure function $f(\sigma;\mathbf{X})$, there holds

$$f(\sigma,\mathbf{X}) \geq F(\mu_k(f(\sigma,\mathbf{X}))) = 0 \tag{5.91}$$

where $F(\mu_k(f(\sigma,\mathbf{X})))$ is some deterministic function of probabilistic moments $\mu_k(f(\sigma,\mathbf{X}))$. The function can be evaluated starting from integration over the probability domain method, the characteristic function differentiation approach, Monte Carlo simulation technique or, alternatively, stochastic perturbation theory. Using the classical second order version of the perturbation technique, zeroth, first and second order equations for Tsai–Hill criteria in the form of

$$f(\sigma;\mathbf{X}) = 1 - \left(\frac{\sigma_1^2}{X^2} - \frac{\sigma_1\sigma_2}{X^2} + \frac{\sigma_1^2}{Y^2} + \frac{\tau_{12}^2}{S^2} \right) \tag{5.92}$$

can be written as

- zeroth order equation:

$$f^0(\sigma;\mathbf{X}) = 1 - \left(\frac{\sigma_1^2}{X^2} - \frac{\sigma_1\sigma_2}{X^2} + \frac{\sigma_1^2}{Y^2} + \frac{\tau_{12}^2}{S^2} \right) \tag{5.93}$$

- first order equations:

$$f^{,r}(\sigma;\mathbf{X}) = -\left(\left(\frac{1}{X^2}\right)^{,r} \sigma_1^2 + \frac{1}{X^2}\left(\sigma_1^2\right)^{,r} - \left(\frac{1}{X^2}\right)^{,r} \sigma_1\sigma_2 - \frac{1}{X^2}(\sigma_1\sigma_2)^{,r} \right.$$
$$\left. + \left(\frac{1}{Y^2}\right)^{,r} \sigma_1^2 + \frac{1}{Y^2}\left(\sigma_1^2\right)^{,r} + \left(\frac{1}{S^2}\right)^{,r} \tau_{12}^2 + \frac{1}{S^2}\left(\tau_{12}^2\right)^{,r} \right) \tag{5.94}$$

- second order equation:

$$f^{(2)}(\sigma;\mathbf{X}) =$$
$$-\left\{ \left(\frac{1}{X^2}\right)^{,rs} \sigma_1^2 + 2\left(\frac{1}{X^2}\right)^{,r} \left(\sigma_1^2\right)^{,s} + \frac{1}{X^2}\left(\sigma_1^2\right)^{,rs} - \left(\frac{1}{X^2}\right)^{,rs} \sigma_1\sigma_2 \right.$$
$$-2\left(\frac{1}{X^2}\right)^{,r} (\sigma_1\sigma_2)^{,s} - \frac{1}{X^2}(\sigma_1\sigma_2)^{,rs} + \left(\frac{1}{Y^2}\right)^{,rs} \sigma_1^2 + 2\left(\frac{1}{Y^2}\right)^{,r} \left(\sigma_1^2\right)^{,s}$$
$$\left. + \frac{1}{Y^2}\left(\sigma_1^2\right)^{,rs} + \left(\frac{1}{S^2}\right)^{,rs} \tau_{12}^2 + 2\left(\frac{1}{S^2}\right)^{,r} \left(\tau_{12}^2\right)^{,s} + \frac{1}{S^2}\left(\tau_{12}^2\right)^{,rs} \right\} Cov\left(b^r, b^s\right) \tag{5.95}$$

Analogous zeroth, first and second order equations can be obtained from Tsai–Wu deterministic criteria, cf. (5.89). Then, the first two probabilistic moments for the failure function $f(\sigma;\mathbf{X})$ can be calculated in the form of expected values

$$E[f(\sigma;\mathbf{X})]=f^{(0)}(\sigma;\mathbf{X})+\tfrac{1}{2}f^{(2)}(\sigma;\mathbf{X}) \tag{5.96}$$

and variances

$$Var(f(\sigma;\mathbf{X}))=\left(f^{,r}(\sigma;\mathbf{X})\right)^2 Var(\mathbf{b}) \tag{5.97}$$

using the relations derived above.

Starting from the first two probabilistic moments , various forms of the function $F(\mu_k(f(\sigma,\mathbf{X})))$ can be proposed which depend generally on the probability density function of input random variables as well as the output PDF of the failure function $f(\sigma;\mathbf{X})$. The following form of F is proposed below:

$$f(\sigma;\mathbf{X})\geq E[f(\sigma;\mathbf{X})]-3\sqrt{Var(f(\sigma;\mathbf{X}))} \tag{5.98}$$

which gives the most accurate result for Gaussian deviates and all symmetric PDF with the same first two probabilistic moments and the fourth order coefficient of concentration greater than 3. By the 'desired result' it is understood that inequality (5.98) holds true with probability almost equal to 1. Let us note that such a function is called an envelope function in stochastic theories of structural reliability.

The probabilistic failure criteria presented above have been examined in terms of the angle θ and axial stress σ being input random variables for the following material properties of the composite X=5.0 GPa, Y=6.0 GPa, S=4.0 GPa for Tsai–Hill criterion and X_t=5.0 GPa, X_c=5.5 GPa, Y_t=6.0 GPa, Y_c=6.6 GPa, S=4.0 GPa in the case of Tsai–Wu model. The variability of the expected values of the input parameters is taken as $E[\theta]$ =0,...,45 and $E[\sigma]$=2.0 GPa,...,6.0 GPa, while their standard deviations are in the range of 10% of the corresponding expected values. All computations are done by the use of the symbolic computation mathematical package MAPLE – zeroth, first and second order failure surfaces are obtained and starting from them the expected values, standard deviations and 'envelope' failure surfaces are plotted. Figures 5.66–5.69 and 5.70–5.73 presented below contain deterministic, probabilistic envelopes, expected values and standard deviations of Tsai–Hill and Tsai–Wu failure surfaces. It is seen that the character of standard deviations for both criteria plots is essentially different from the other surfaces.

Analysing the results plotted in Figures 5.66–5.73 it should be underlined that deterministic surfaces are quite close to their expected values (see (5.96)). It is caused by the fact that the coefficient of variation of both input random variables is relatively small. Further, it is observed that the 'envelope' failure surfaces for both Tsai–Hill and Tsai–Wu criteria have generally the same character as the corresponding deterministic and expected values. However, essentially smaller values generally confirm its usefulness in the probabilistic analysis of composite failure and should be studied further in detail. Especially valuable would be the application of the methodology proposed in the case of full statistical information on composite strength properties and the external load applied.

Finally, it should be underlined that the symbolic approach to stochastic perturbation analysis makes possible any finite order computations of probabilistic moments of the output. Due to this fact, precise numerical studies on model convergence for different perturbation orders, various PDF of input variables and their probabilistic parameters should be carried out.

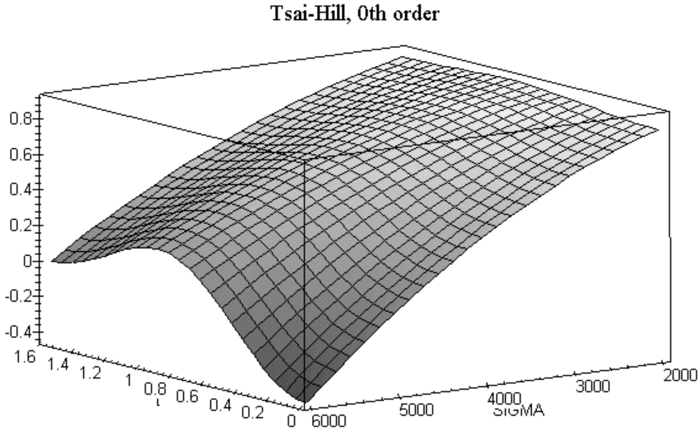

Figure 5.66. Tsai–Hill deterministic failure surface

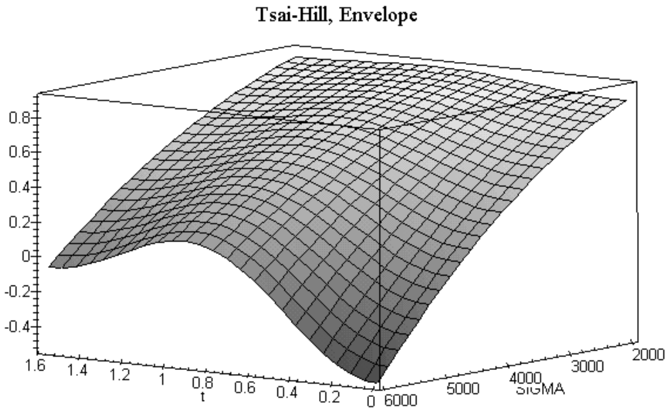

Figure 5.67. Tsai–Hill 'envelope' failure surface

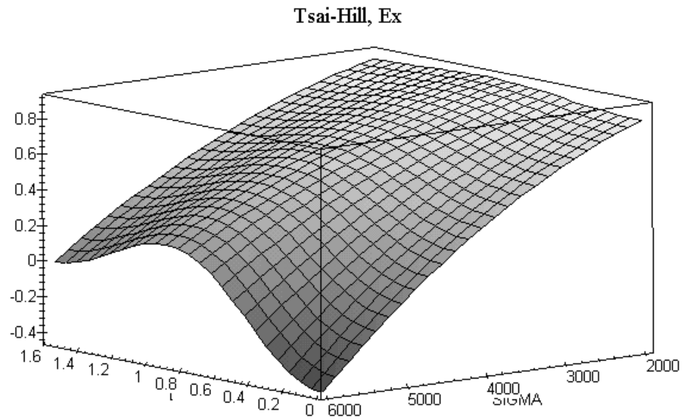

Figure 5.68. Expected values for Tsai−Hill failure surface

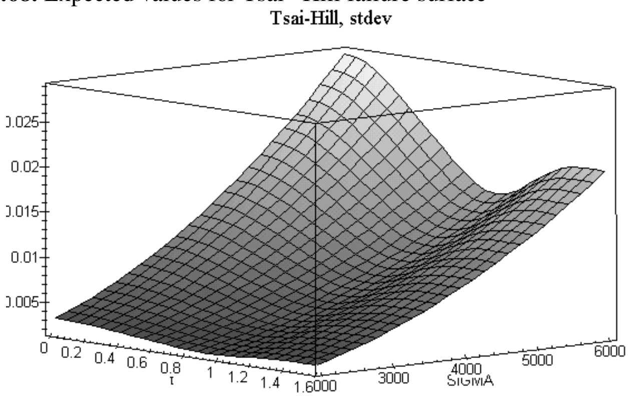

Figure 5.69. Standard deviations of Tsai−Hill failure surface

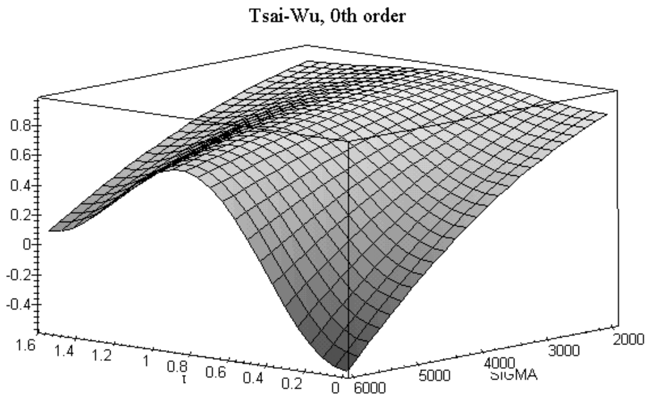

Figure 5.70. Tsai−Wu deterministic failure surface

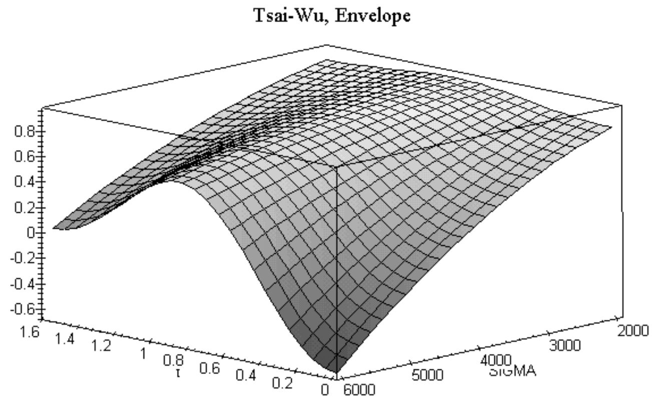

Figure 5.71. Tsai – Wu 'envelope' failure surface

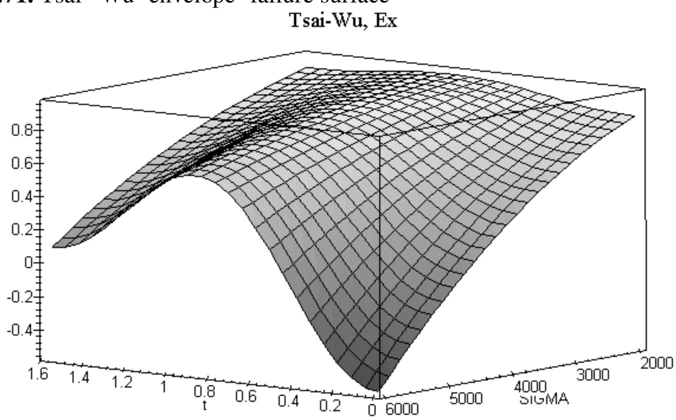

Figure 5.72. Expected values for Tsai – Wu failure surface

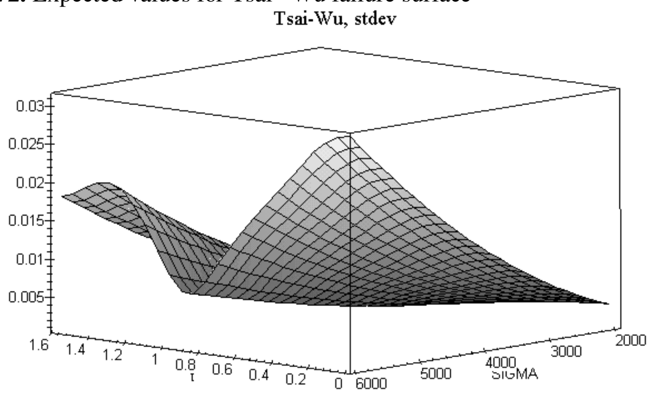

Figure 5.73. Standard deviations of Tsai – Wu failure surface

5.5 Concluding Remarks

The whole variety of mathematical and computational tools shown above makes it possible to analyse efficiently ordinary and cumulative deterministic and stochastic fatigue processes in different composite materials. Some local and global models are mentioned and the deterministic or stochastic techniques together with the approaches which enable randomisation of classical deterministic techniques to obtain at least the first two probabilistic moments of the structural response. For this purpose, most established composite oriented fatigue theories are classified and listed here. Next, the application of the perturbation–based SFEM has been demonstrated for various aspects of the fatigue process computational modelling to the W–SOTM reliability analysis, starting from direct FEM simulation in conjunction with fracture phenomena.

An alternative computational technique (MCS) is shown using the example of homogenisation analysis for a fibre–reinforced composite with stochastic interface defects simulating interface fatigue. Most of the computational illustrations presented above show, which is intuitively clear, that the expected values of structural functions decrease together with fatigue process progress. In the same time, the second order probabilistic characteristics (standard deviations, variances or coefficients of variation) increase together with the increase of fatigue cycle number, which means that the random uncertainty measure is increasing during the entire process.

The probabilistic modelling of composite materials fatigue processes summarised and proposed in this chapter is still an open question due to the fact that the area of composite material applications as well as the relevant technologies is still extending and because of the developments of the stochastic mechanics itself. The stochastic second or higher order perturbation theory for various problems shown above is very fast in randomisation of composite fatigue theories and in computational modelling. However, it is not sufficiently efficient in numerical simulation of engineering systems with increasing standard deviations of input structural parameters. The simulation methods based on the MCS approach are computationally exact, but not very effective in simple approximation of the probabilistic moments of the composite state functions, their failure criteria and the additional reliability index. Further usage of stochastic differential equations computer solvers [149] in conjunction with the FEM is recommended to include full stochastic nature of crack initiation and detection into the model.

An essential minor point of the up–to–date fatigue analysis methods (both deterministic and stochastic) is the lack of microstructural effects in the final formulae; some work is done for laminated structures. However interface phenomena in fibre–reinforced composites and stochastic microstructural problems in all composites are not included in the analysis until now. Finally, the lack of systematic sensitivity analysis of various models is observed, which makes it impossible to find a reasonable compromise between complexity of the fatigue analysis approach, probabilistic treatment of various phenomena resulting in cumulative damage and applied mathematical and numerical techniques. Such a sensitivity analysis should be carried out treating the expected values and higher order probabilistic moments of structural composite parameters as design variables, which seems to be necessary considering the application of random variables and fields in this area.

5.6 Appendix

Various fatigue models are collected below to give the overview of the capabilities of this analysis for both homogeneous and heterogeneous structures; they are listed according to the subject classification presented in this chapter.
A. Fatigue cycles number analysis − determine N:
1. Madsen (power law function) [244]:

$$N = KS^{-m} \tag{A5.1}$$

S is stress amplitude, K,m are some material constants;
2. Boyce and Chamis [42]:

$$N = 10\exp\left\{\log N_{MF} - \left[\left(\log N_{MF} - \log N_{MO}\right)\right]\left[\frac{S}{S_0\left[\dfrac{T_F - T}{T_F - T_0}\right]^n\left[\dfrac{S_F - \sigma}{S_F - \sigma_0}\right]^m}\right]^{\frac{1}{q}}\right\} \tag{A5.2}$$

N_{MF} − final cycle, N_{MO} − reference cycle, S − fatigue strength, S_0 − reference fatigue strength, T_F − final temperature, T_0 − reference temperature, T − current temperature, σ − current mean stress, σ_0 − reference (residual) stress, n,q − empirical parameters;
3. Caprino, D'Amore and Facciolo [53]:

$$N = \sqrt[\beta]{1 + \frac{1}{\alpha(1-R)}\left\{\frac{\gamma}{\sigma_{\max}}\left|\ln\left(1 - f_n(N)\right)\right|^{\frac{1}{\sigma}} - 1\right\}} \tag{A5.3}$$

$f_n(N)$ − probability of failure; γ,σ − scale parameter (characteristic strength) and the shape parameter of the Weibull distribution of the static strength; R − given stress ratio; $\sigma_{\max}$ − maximum stress level; α, β − constants from experiments.

B. Stiffness reduction models:

1. Whitworth [365]:

$$\frac{dE(N)}{dN} = -\frac{Df^{a}(E_0, S)}{aE^{a-1}(N)} \tag{A5.4}$$

$E(n)$ – residual modulus after n fatigue cycles, E_0 – initial modulus, $N=n/N^*$ – ratio of applied cycles to fatigue life; S,a,D – some constants, $f(E_0,S)$ – some function of E_0,S, i.e. $C\left[E_0 - \frac{S}{e_f}\right]$, e_f – constant depending on overall strain at failure;

2. Hansen [127]:

$$\frac{E}{E_0} = 1 - \beta\,, \;\; \beta = A\int_0^N \left(\frac{\varepsilon_e}{\varepsilon_0}\right)^n dN \tag{A5.5}$$

A – some constant, ε_e – effective strain level, ε_0 – damage strain where

$$\dot{\beta} = \frac{d\beta}{dN} = A\left(\frac{\varepsilon_e}{\varepsilon_0}\right)^n \tag{A5.6}$$

3. Bast and Boyce (creep component for the stiffness reduction) [20]:

$$\frac{S}{S_0} = \left[\frac{t_u - t_0}{t_u - t}\right]^{-v} \cong \left[\frac{10^6 - 0.25}{10^6 - t}\right]^{-v} \tag{A5.7}$$

t_u – ultimate strength of creep hours when rupture strength is very small, t_0 – reference number of creep hours where rupture strength is very large, t – current number of creep hours, v – empirical material constant for the creep effect.

C. Fatigue crack growth analysis ($\frac{da}{dN}$) - *deterministic methods* (Yokobori [379]):

1. Liu (energy approach)

$$\alpha_1\left(\frac{\Delta K}{\sigma_{sy}}\right)^2 \tag{A5.8}$$

2. Paris (energy approach)

$$\frac{\alpha_2}{l_2}\left(\frac{\Delta K}{\sigma_{sy}}\right)^4 \tag{A5.9}$$

3. Raju (energy approach)

$$\alpha_3 \frac{\Delta K^4}{\sigma_{sy}^2\left(K_{Ic}^2 - K_{\max}^2\right)}\,; K_{\max} << K_1 \tag{A5.10}$$

	$\alpha_3 \dfrac{\Delta K^4}{\sigma_{sy}^2 K_{Ic}^2}$	
4. Cherepanov (energy approach)	$\alpha_4 \dfrac{\Delta K^4 E}{\sigma_{sy}^3 K_{Ic}^2}$	(A5.11)
5. Rice (crack opening displacement – COD)	$\dfrac{\alpha_5}{l_5}\left(\dfrac{\Delta K}{\sigma_{sy}}\right)^4$	(A5.12)
6. Weertman (continuous dislocation formalism)	$\alpha_6 \dfrac{\Delta K^4}{\gamma E \sigma_{sy}^2}$	(A5.13)
7. Weertman, Mura and Lin (continuous dislocation formalism)	$\alpha_7 \dfrac{\Delta K^4}{\gamma_p \mu \sigma_a^2}$	(A5.14)
8. Lardner (COD)	$\alpha_8 \dfrac{\Delta K^2}{E\sigma_{sy}}$	(A5.15)
9. Schwalbe (COD)	$\alpha_9 \dfrac{\Delta K^2}{E\sigma_{sy}}$	(A5.16)
10. Pook and Frost (COD)	$\alpha_{10}\left(\dfrac{\Delta K}{E}\right)^2$	(A5.17)
11. Tomkins (skipband decohesion)	$\dfrac{\pi}{8}\left(\dfrac{\Delta K}{\sigma_{sy}}\right)^2\left(\dfrac{\Delta\sigma}{\sigma_0}\right)^{\frac{1}{\beta}}$	(A5.18)
12. McEvily (semi-experimental approach with COD)	$\dfrac{(\Delta K - \Delta K_{TH})^2}{\sigma_{sy} E} f(\Delta K, K_{1c}, K_{\max})$	(A5.19)
13. Donahue *et al.* (COD)	$\alpha_{11} \dfrac{\Delta K^2}{\mu \sigma_a}$	(A5.20)
14. Yokobori I (nucleation rate process approach)	$\alpha_{12}\left(\dfrac{\Delta K}{\gamma E}\right)^{1/2\xi kT}$	(A5.21)
15. Yokobori II (nucleation rate process approach)	$\alpha_{13}\left(\dfrac{\Delta K}{\sqrt{s}\sigma_{cy}}\right)^{2\beta/(1+\beta)}\left(\dfrac{b\sigma_{cy}^2}{\gamma E}\right)^{1/2\xi kT}$	(A5.22)
16. Yokobori III (dislocation approach)	$\alpha_{14}\left(\dfrac{\Delta K}{\sqrt{s}E}\right)^{\frac{(m+1)^2}{m+2}}$	(A5.23)
17. Yokobori IV (dislocation approach)	$\alpha_{15}\left(\dfrac{\Delta K}{\sqrt{s\gamma}}\right)^{\frac{2\beta}{1+\beta}\frac{(m+1)^2}{m+2}+\frac{1}{1+\beta}}\left(\dfrac{\sigma_{cy}}{E}\right)^{\frac{(m+1)^2}{m+2}}$	(A5.24)

where α_i, i=1,15 denote some experimentally determined material constants;

18. Yokobori V (monotonic yield strength dependence) $$B\left(\frac{\Delta K}{\sqrt{s}\sigma_c}\right)^n \qquad \text{(A5.25)}$$

19. Paris–Erdogan [280]:

$$C(\Delta K)^m = C\left[Y(a)\Delta\sigma\sqrt{\pi a}\right]^m \qquad \text{(A5.26)}$$

$Y(a)$ – geometry factor, $\Delta\sigma$ – stress range, C, m – some material constants;

20. Ratwani–Kan [296]:

$$C\left(\tau_{zma} - \tau_{zmi} - \tau_{th}\right)^{n_1} b^{m_1} \qquad \text{(A5.27)}$$

τ_{zmi} – minimum interlaminar shear stresses, τ_{zma} – maximum interlaminar shear stresses, τ_{th} – interlaminar threshold shear stress range, C, n_1, m_1 – material constants, b – delamination length;

21. Wang–Crossman:

$$\alpha\left[\frac{C_e(a)t\sigma_m^2}{G_c E^2}\right] \qquad \text{(A5.28)}$$

G_c – critical strain energy rate; σ_m – applied load, E – elastic modulus, a – delamination width; t – ply thickness;

22. Forman *et al.* [101]:

$$\frac{C(\Delta K)^m}{(1-R)K_C - \Delta K}; \qquad R = \frac{K_{\min}}{K_{\max}} \qquad \text{(A5.29)}$$

where C, m are the material constants with $m \approx 3$ for steels and $m \approx 3\text{-}4$ for alluminium alloys;

23. Donahue *et al.* [82] for $\Delta K \to \Delta K_{th}$ obtained

$$C\left[\Delta K - \Delta K_{th}\right]^m \qquad \text{(A5.30)}$$

24. McEvily and Groeger [247]

$$\frac{A}{E\sigma_Y}\left[\Delta K - \Delta K_{th}\right]^2\left[1 + \frac{\Delta K}{K_{IC} - K_{\max}}\right] \qquad \text{(A5.31)}$$

where σ_Y denotes the yield stresses of the specimen, A is an environment sensitive material parameter and K_{IC} is a plane strain fracture toughness.
25. Experimentally based law for combined mode I and mode II loadings proposed by Roberts and Kibler [302], where crack growth is obtained as

$$C(\Delta K_e)^m, \qquad K_e = \left(K_I^4 + 8K_{II}^4\right)^{\frac{1}{4}} \tag{A5.32}$$

26. Hobson [137] proposed one of the first quantitative models to describe short fatigue crack growth in terms of a microstructural parameter d assumed as a material characteristic

$$Ca^{\alpha}(d-a)^{1-\alpha};\ a \le d \tag{A5.34}$$

where α, C are empirical constants (C depends on both material and loading parameters – Young modulus, yield stress and the applied cyclic stress);

27. Kitagawa–Takahashi curve: the LEFM (linear elastic fracture mechanics) approach determining the condition describing the stress level ΔK_{th} when the cracks can grow

$$\Delta K_{th} = Y\Delta\sigma\sqrt{\pi a} \tag{A5.35}$$

Let us recall that the LEFM approach is invalid when the small–scale yielding conditions are exceeded $\Delta\sigma \ge \frac{2}{3}\sigma_{cy}$ where σ_{cy} is the cyclic yield stress;

28. Priddle law [290]:

$$C\left(\frac{\Delta K}{K_F - K_{\max}}\right)^2 \tag{A5.36}$$

C – growth resistance, K_F – critical value for the stress intensity factor;

D. Fatigue crack growth analysis – determination of $\frac{da}{dN}$ (*some stochastic methods)*

$$\frac{da(t)}{dt} = Q(\Delta K, K_{\max}, S, A, R)X(t) = Q(a)(\mu + Y(t)) \tag{A5.37}$$

$a(t)$ – random crack size, Q – some nonnegative function, ΔK – stress intensity factor range, $K_{\max}$ – maximum stress intensity factor, $X(t)$ – nonnegative random process, $Y(t)$ – random process with 0 mean;

1. Ditlevsen and Sobczyk [80]:

$$\frac{da(t)}{dt} = a^p X(t,\gamma) \tag{A5.38}$$

p = 1,3/2,2 (experimental), $X(t)$ – Gaussian white noise, process with finite correlation time;
2. Lin and Yang [234]:

$$X(t,\gamma) = \sum_{k=1}^{N(t)} Z_k w(t,\tau_k) \tag{A5.39}$$

$N(t)$ – homogeneous Poisson counting process, τ_k – arrival time of kth pulse, Z_k – random amplitude of kth pulse with the following synergistic sine hyperbolic functional form:

$$\left[\frac{da(n)}{dn}\right]' = 10^{C_1 \sinh\left|C_2\left(\log \Delta K + C_3\right)\right| + C_4} \tag{A5.40}$$

$a(n)$ – half crack length, C_i – some parameters
– randomized form:

$$\frac{da(n)}{dn} = X(n)\left[\frac{da(n)}{dn}\right]' \tag{A5.41}$$

3. Spencer *et al.* [327]:

$$\frac{da(t)}{dt} = Q(a)10^Z,\ \frac{dZ}{dt} = -\xi Z + G(t),\ a(0) = a_0,\ Z(0) = Z_0 \tag{A5.42}$$

where G(t) – stationary Gaussian white noise, $Z(t)$ – nonstationary random process; the Pontriagin–Vitt equation is used

$$-nT^{n-1} = Q(a_0)10^{z_0}\frac{\partial T^n}{\partial a_0} - \xi z_0 \frac{\partial T^n}{\partial z_0} + \pi S_0 \frac{\partial^2 T^n}{\partial z_0^2},\ n=1,2,... \tag{A5.43}$$

with the boundary conditions:

$$T^0(a_0, z_0) \equiv 1, \qquad T^n(a_0, z_0) \to 0 : z_0 \to \infty \tag{A5.44}$$

$$\forall z_0 : T^n(a_c, z_0) = 0, \qquad \frac{\partial T^n(a_0, z_0)}{\partial z_0} \to 0 : z_0 \to -\infty \tag{A5.45}$$

Fatigue damage function based model − calculation of $\frac{dD}{dN}$:

1. Palmgren−Miner model [299]:

$$D = \frac{n}{N} \tag{A5.46}$$

n − number of fatigue cycle, N − number of cycles to failure;

2. Modified Palmgren−Miner model:

$$D = \left(\frac{n}{N}\right)^{C} \tag{A5.47}$$

C − constant independent of applied stress; some probabilistic aspects of this model can be found in [254];

3. Shanley model:

$$D = CS^{kb} n \tag{A5.48}$$

S − applied stress, C,K − constants, b − slope of central position of S−N curve;

4. Marco−Starkey model:

$$D = \left(\frac{n}{N}\right)^{C_i} \tag{A5.49}$$

C_i>1 − stress dependent constant;

5. Henry model:

$$D = \frac{(S_t - S_t')}{S_t} \tag{A5.50}$$

S_t − fatigue of virgin specimen, S_t' − fatigue limit after damage;

6. Corten−Dolan model:

$$D = mcn^{\alpha} \tag{A5.51}$$

m − number of damage nuclei, c,a − function of stress condition; α − some constant;

7. Gatt model:

$$D = (S_t - S_t')^{\alpha} \quad \text{(A5.52)}$$

8. Marin model:

$$S^k N = C \quad \text{(A5.53)}$$

9. Manson model:
− for crack initiation:

$$D = \frac{n}{N_I} \quad \text{(A5.54)}$$

− for crack propagation:

$$D = \frac{n}{N_P} \quad \text{(A5.55)}$$

10. Owen−Howe model:

$$D = B\left(\frac{n}{N}\right) - C\left(\frac{n}{N}\right)^2, \quad \text{(A5.56)}$$

B,C − some constants;
11. Srivatsavan−Subramanyan model:

$$D = \frac{\log N_t - \log N}{\log N_t - \log n} \quad \text{(A5.57)}$$

12. Lemaitre−Plumtree model:

$$D = 1 - \left(1 - \frac{n}{N}\right)^a \quad \text{(A5.58)}$$

$a = \dfrac{1}{p+1}$ strain controlled; $a = \dfrac{1}{c+p+1}$–stress controlled; p,c–material constants
13. Fong model [100]:

$$D = \frac{\exp(kx) - 1}{\exp(k) - 1} \quad \text{(A5.59)}$$

where k represents damage trend;
14. Cole model:

$$A_D = A - C \quad \text{(A5.60)}$$

A_D – attenuation due to damage, A – total attenuation, C – attenuation of virgin specimen;
15. Fitzgerald–Wang model:

$$D = 1 - \frac{E}{E^*} \tag{A5.61}$$

E – modulus at a fatigue cycle; E^* – reference modulus;
16. Wool model:

$$-\frac{dD}{dt} = kD^a \tag{A5.62}$$

17. Chou model:

$$D = \Delta F(n) \tag{A5.63}$$

18. Hwang–Han model I [143]:

$$D = \frac{F_0 - F(n)}{F_0 - F_f} = \left(\frac{n}{N}\right)^c \tag{A5.64}$$

F_0 – undamaged, F_f – damaged modulus;
19. Hwang–Han model II [144]:

$$D = \frac{\varepsilon(n)}{\varepsilon_f} = \frac{r}{1 - Kn^c} \tag{A5.65}$$

ε_f – failure strain;
20. Hwang–Han model III:

$$D = \frac{\varepsilon(n) - \varepsilon_0}{\varepsilon_f - \varepsilon_0} = \frac{r}{1-r}\frac{n^c}{B - n^c} \tag{A5.66}$$

21. Morrow approach [257]:

$$D_i = \frac{n_i}{N_i}\left(\frac{S_i}{S_m}\right)^d \tag{A5.67}$$

S_i – amplitude of stress causing fatigue damage, S_m – maximum stress amplitude, n_i – number of stress peak at level S_I, d – plastic work interaction exponent, N_i – number of stress peak to the failure if S_i =const.;

22. Morrow approach with different cycles:

$$D(t) = \sum_{i=1}^{n(t)} \frac{1}{N_i} \left(\frac{S_i}{S_m(t)} \right)^d \tag{A5.68}$$